THE APPLIED ORIENTATION OF THE PHYSICS COURSE AS AN EFFECTIVE TOOL FOR FORMING THE PROFESSIONAL COMPETENCE MODEL OF FUTURE TECHNOLOGICAL ENGINEERS

Anatolii Biliuk[1]
Olena Diachynska[2]

DOI: https://doi.org/10.30525/978-9934-26-298-2-1

Abstract. Reliability of structures is the most important problem in modern mechanical engineering. Its solution poses the task of creating materials with high stable physical, mechanical, chemical and other properties. The materials that make up the basis of structures are, as a rule, operated in variable fields of various nature (mechanical, temperature, etc.), therefore they continuously change their properties. In this regard, progress in the field of mechanical engineering cannot be achieved without full knowledge of the real structure of materials, without a deep understanding of the microprocesses that occur in the materials during their processing and operation.

Therefore, *the purpose* of the work is to describe methods and techniques for determining damping, structural and mechanical characteristics of materials and to evaluate the nature of their changes under the influence of temperature, time and force factors.

The most promising non-destructive physical research *methods* include the method of mechanical spectroscopy (internal friction) and the microhardness method. With the help of the method of mechanical spectroscopy, it is possible to reliably determine such seemingly different properties of materials as the ability to dampen vibrations arising during the

[1] Candidate of Physical and Mathematical Sciences,
Associate Professor of the Department of Physics and
Teaching Methods of Physics, Astronomy,
Vinnytsia State Pedagogical University named after Mykhailo Kotsyubynskyi, Ukraine;
Associate Professor of the Department of Mathematics,
Physics and Computer Technologies,
Vinnytsia National Agrarian University, Ukraine
[2] Assistant of the Department of Mathematics, Physics and Computer Technologies,
Vinnytsia National Agrarian University, Ukraine

operation of machine parts, the diffusion mobility of atoms in the crystal lattice and along dislocations. Internal friction (IF), which characterizes the ability to dissipate the energy of mechanical vibrations with a large and small amplitude in the material, can often be unambiguously associated with the number and mobility of dislocations and point defects of the crystal lattice. At the same time, it allows you to assess the material's susceptibility to another consequence, creep and grain boundary relaxation. Processes such as separation and dissolution of residual phases, relaxation, rest, hardening and tempering, dispersion hardening, plastic deformation and deformation aging and return have been successfully studied for many years by the method of internal friction. IF not only makes it possible to determine damping, structural and mechanical characteristics, but also to follow the nature of their changes in the fields of various nature [1–4]. Microhardness, which characterizes the energy of the interatomic bond of the crystal, its mechanical strength or the resistance of the crystal lattice to large plastic deformations and destruction, was chosen as a controlling characteristic in the study of the results.

The research *results* showed that thermal cycling leads not only to the for-mation of high density dislocations in alloys, but also to their redistribution into polygonal walls. This is due to the fact that the available impurities, their complexes or separate dispersed allocations significantly block the newly formed dislocations and the already formed substructure, and thus increase its thermal stability and increase the heat resistance of the material. At the same time, as the strength characteristics increase, the damping properties are not significantly lost.

Value/originality. Application of thermocycling under load is possible not only for materials made of dispersion-hardening alloys, which serve as raw materials for technology and industry, but also for finished parts and technical structures made of them. This will simplify the processing technology, reduce energy consumption and allow to obtain a significant economic effect.

1. Introduction

Reliability of structures is the most important problem in modern mechanical engineering. Its solution poses the task of creating materials with high stable physical, mechanical, chemical and other properties.

The materials that make up the basis of structures are, as a rule, operated in variable fields of different nature (mechanical, temperature, etc.) and intensity, therefore they continuously change their properties. In this regard, progress in the field of mechanical engineering cannot be achieved without full knowledge of the real structure of materials, without a deep understanding of the microprocesses that occur in the material during their processing and operation.

The most promising physical methods of research include the method of mechanical spectroscopy (the method of internal friction), with which it is possible to reliably determine such seemingly different properties of materials as the ability to dampen vibrations arising during the operation of machine parts, the diffusion mobility of atoms in the crystal lattice and along dislocations. Internal friction (IF), which characterizes the ability to dissipate the energy of mechanical vibrations with a large and small amplitude in the material, can often be unambiguously associated with the number and mobility of dislocations and point defects of the crystal lattice. At the same time, it allows you to assess the material's susceptibility to another consequence, creep and core boundary relaxation. Processes such as separation and dissolution of residual phases, relaxation, rest, hardening and tempering, dispersion hardening, plastic deformation and deformation aging and return have been successfully studied for many if years by the method of internal friction. IF not only makes it possible to determine damping, structural and mechanical characteristics, but also to follow the nature of their changes in the fields of various nature [1–4].

Internal friction appears in two categories – as a phenomenon specifically related to one or another process, and on the other hand – after establishing an unequivocal connection between the amount of internal friction and a given mechanism of energy absorption – as a physical research method.

Reconstruction of the dislocation systems by the method of mechanical and thermal processing leads to the formation of substructures, and at the same time, to the appearance of new quality characteristics of the material – strengthening, high damping capacity.

The study of internal friction in substructurally strengthened metals and alloys is a difficult but necessary task both experimentally and theoretically.

2. Mechanical spectroscopy of metals and alloys

Losses of acoustic energy measured directly in the process of deformation can be divided into two groups. The first includes losses that reflect the evolution of the dislocation structure, and the second includes losses that are spent on the deformation process itself. Losses of the first type will be called structural losses. They do not depend on (if aging processes are neglected) whether deformation is taking place at the moment, but depend on the structure formed before the deformation. Losses of the second type can be called dynamic, since they exist while the process of plastic friction takes place. These losses are due to the fact that, in comparison with the carriers of plastic deformation, which are at rest, the carriers of plastic deformation, moving in translation, have additional inelasticity.

2.1. Structural internal friction

The theoretical description of the structural internal friction and problems related to it are reflected in a large number of articles, reviews and monographs. A significant part of the theories is based on the basic string model [5; 6] of Koehler-Granato-Lyukke (KGL). In this model, the dislocation is considered as a string fixed at some points by local stoppers. At small oscillation amplitudes, when the dislocation does not break away from the attachment points, the internal friction does not depend on the amplitude. It is caused only by the viscous braking of oscillating dislocations due to their interaction with the elementary lattice excitations (phonons, electrons). The Granato-Lyukke theory [6] predicts a maximum of amplitude-independent internal friction at sufficiently high frequencies (tens of *MHz* and higher). For frequencies below the maximum, the theory gives the following formulas [6]:

$$\delta_1 = k_1 \Lambda l^4 \omega B, \tag{2.1}$$

$$\left(\Delta M / M\right)_1 = k_2 \Lambda l^2, \tag{2.2}$$

where δ_1 i $\left(\Delta M / M\right)_1$ – amplitude-dependent decrement and defect of the modulus of elasticity, respectively ($\Delta M = M - M_d$, here M – is the modulus of elasticity of an ideal crystal, and M_d – is the modulus of a crystal with dislocations), Λ – density of dislocations, l (L_{av}) – average length of the dislocation segment between anchoring points, ω – cyclic frequency of oscillations, B – anchoring constant of viscous braking of dislocations,

$k_1(C_1)$ and $k_2(C_2)$ – are coefficients that depend on the linear tension of the dislocation and on the distribution of dislocation segments along their lengths (here and in the following formulas the orientation factor is omitted, which takes into account the polarization of the sound wave relative to the sliding system).

When the amplitude of oscillations increases, the decrement δ can be represented as a sum δ_1 and an amplitude-dependent part δ_h (ADIF). In the theories of ADIF based on the KGL model, it is assumed that the amplitude dependence is a consequence of the hysteresis movement of dislocations in the force fields of point defects by the "detachment-reattachment" mechanism from the same stoppers in each of the half periods of oscillations. At the same time, it is considered that the dislocation overcomes only one row of weak attachment points, since it cannot break away from strong stoppers (nodes of the dislocation grid, etc.). There are other theories of ADIF, in which the dislocation passes through several rows of stoppers and even long-range fields of internal stresses. According to Asano's classification [7], theories of the first type are called detachment theories, and the second are called friction theories, since the mobility of dislocations, according to these theories, is controlled by some effective force of friction. There are other models of the movement of dislocations that contribute to IF (for example, the Alefeld model [8]). The behavior of IF under the action of an additional static load in certain cases according to [8] is used as an identifier of one or another mechanism.

2.2. Dynamic losses

Later, a theoretical analysis of the dynamic losses was carried out [9-16] using specific initial equations of the plastic deformation. During the calculations, it was assumed that the rate of the plastic deformation is determined by the ratio:

$$\dot{\varepsilon} = \dot{\varepsilon}_0 exp\left[-H(\sigma)/(kT)\right], \tag{2.3}$$

where $\dot{\varepsilon}_0$ – is a constant, T – temperature, k – Boltzmann's constant, $H(\sigma)$ – the activation energy of the deformation process, which depends on the tension, and the problem is solved for the case when the relationship between H and σ is linear:

$$\dot{\varepsilon} = \dot{\varepsilon}_0 \left[-\frac{H_0 - V(\sigma - \sigma_1)}{kT} \right], \tag{2.4}$$

here V – activation volume, H_0 – constant, σ_1 – internal stress in the crystal. If we assume that the external stress contains a periodically variable component $\sigma_v = \sigma_e \cos(\omega t)$, we obtain an expression for the rate of deformation under the joint action of static and dynamic stresses:

$$\dot{\varepsilon}_{v+s} = \dot{\varepsilon} exp\left[V_{\sigma_v} / kT \right], \tag{2.5}$$

where $\dot{\varepsilon}$ – is the rate of deformation in the absence of periodic stress, which is given by formula (2.4). The energy of oscillations, which is lost due to plastic deformation per unit volume per period, is equal to:

$$\Delta W = \int_0^{2\pi/\omega} \sigma_v \dot{\varepsilon}_{v+s} dt. \tag{2.6}$$

In [6], we consider V_{σ_v} / kT the value to be small, so we limit our-selves to the linear term when expanding the exponent [5] into a series:

$$\dot{\varepsilon}_{v+s} = \varepsilon \left[1 + V_{\sigma_v} / kT \right]. \tag{2.7}$$

Then $\Delta W = \pi V_{\sigma_0^2} \dot{\varepsilon} / \omega kT$. By definition, the decrement of oscillations is equal to half the ratio of the energy dissipated over a period in a unit of volume to the energy W received in the same volume and for the same time:

$$\delta = \Delta W / (2W) \tag{2.8}$$

Assuming $W = 0,5\sigma_0^2 / M$, for dynamic decrement, we get [6]:

$$\delta_d = \pi M V \dot{\varepsilon} / (\omega kT). \tag{2.9}$$

According to (2.9), the decrement does not depend on the amplitude of the oscillations. But this is a consequence of using the approximate expression (2.7). In the general case, it is necessary to integrate (2.5), which was done in Kaiser's theory [9; 10], he obtained a dependence δ_d on the amplitude. For this, it is necessary to take into account that the dipole oscillatory load, which is applied in the process of quasi-static deformation, can affect the process of deformation itself and cause an acoustoplastic effect. This effect is manifested both in the creep mode, when the rate of deformation increases under the influence of vibrations (the Archbutt effect [16]), and during active deformation at a constant

rate, when the oscillating load reduces the stress of the plastic flow (the Blag-Langenecker effect [17]).

Thus, the total loss of the vibrational energy in the process of deformation consists of the static (structural) and dynamic losses. According to (2.1), the static losses in the low-frequency region (below the Granato-Lyukke maximum) increase proportionally to the frequency [6], that is, the contribution of the dynamic losses in relation to the static losses should decrease with frequency ω^{-2}.

2.3. Low-frequency internal friction

Most of the data in the low-frequency range were obtained during the de-formation of aluminum and its alloys [10; 12–14]. Iron [14], nickel [18], copper [11; 12], zinc [19], silver [19], brass [11] were also studied. Measurements were carried out both during active deformation [9; 10–13; 20] and during creep [10; 18]. Experimental data mainly confirm the dependence of the decrement on the rate of deformation and frequency in accordance with the theory of dynamic IF. When the deforming device is stopped, the decrement drops almost instantly to a level not much higher than in the undeformed sample [20]. With an increase in the rate of deformation, a linear increase in damping is observed [6; 10; 11; 14]. A wide range of velocities was studied in papers where IF was measured during jump-like deformation (the Portvain-Le Chatelier effect [9]). It was possible to overlap 3 orders and no deviations from linearity were detected (Figure 1.1. a). The inverse proportionality of the decrement to the oscillation frequency was also observed in other works [11; 14], but it was most successfully done in [13] with the help of a specially developed technique. The frequency varied from 0,1 to 320 Hz. At the lowest frequencies (1 Hz and below) at relatively high defor-mation rates (of the order of $10^{-3} c^{-1}$), a maximum absorption of vibra-tion energy is observed (Figure 1.1. b shows data for the imaginary part of the elastic compliance), which follows from the theory [13].

A decrease in IF with amplitude was also observed in [11; 12]. Measurements for only the first few periods show a growing dependence for aluminum (Figure 1.1. c) and no dependence for copper [12]. In the region of large amplitudes, the theory [9] ceases to be valid. Amplitude spectra look quite complex, and for their decipherment the authors [20] suggest taking into account not only dynamic, but also structural IF.

The contribution of low-frequency IF can also be registered in the area of small amplitudes. For example, in [21], changes in IF at fixed creep, when neither the rate of deformation nor the frequency change, were explained from the point of view of the Granato-Lyukke theory.

Structural changes during deformation can cause IF maxima. For example, during the creep of zinc polycrystals, peaks were observed, the position and magnitude of which depended on the grain size. In [19], IF was studied in the process of aluminum creep. At temperatures of 373 K and 423 K in polycrystals, maxima were observed on the dependence of IF on the deformation time [19], the authors connected these maxima (and proved this with electron microscopy data) with the rearrangement of the dislocation structure during the transition from one stage to another. At $T = 297\,K$ and $T = 683\,K$ the maximum was not observed (or it did not appear at long intervals of time [22]), the decrement and defect of the modulus decreased with time similar to the creep rate curve, which qualitatively agrees with the theory [9; 10; 13] and experiments [13], although the authors of [22] associate changes in IF and modulus of elasticity with changes in the distribution function of the lengths of dislocation segments. Note that the authors of [22] observed a maximum at $T = 463\,K$ only in a single crystal, and there was no maximum in a polycrystal.

Unsteady behavior of IF was also recorded during the deformation of the $Fe - 0,03\,wt.\%$ C alloy, in which the diagram $A - \mu$ demonstrated a tooth and a temporary current on the platform of fluidity. Since during damping measurements the deforming machine was stopped (for approximately 30 s), the observed non-stationarity cannot be explained on the basis of theories [9–14]. It was concluded that the oscillating character of the IF is related to the fluctuations of the density of dislocations relative to its limiting value at the yield point.

Thus, in most experiments on the registration of low-frequency IF in the process of plastic deformation, the main contribution to the absorption of vibrational energy is provided by the mechanism of dynamic losses. The decrement δ_d of oscillations due to this mechanism can have the following characteristic features:

a) proportionality of the rate of deformation;

b) inverse proportionality to the frequency of oscillations;

c) anomalous amplitude dependence (as ε the decrement increases, it decreases) –72 to + 130°C.

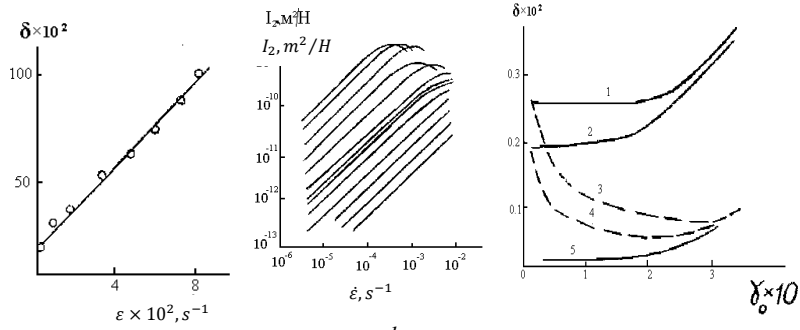

a *b* *c*

Figure 2.1. a – Dependence of the decrement of torsional vibrations on the rate of deformation of α – brass, b – Dependence of the imaginary part of the elastic compliance on the rate of deformation, c – Amplitude dependences of the decrement of torsional vibrations, measured in the process of deformation of the *Al* polycrystal at different rates: 1, 2 – measurements for the first few periods of oscillations with a given amplitude; 3, 4 – the established regime [9]

3. Physical methods, methodology and research objects

3.1. Materials and conditions of the experiment

Dispersion-hardening alloys (DHA) based on aluminum are promising materials in various fields of technology and, first of all, in aviation and space technology. It is known that the properties of DHA are determined both by the properties of the components and by their interaction with each other and defects in the crystal structure of the material. Various thermomechanical treatments are used to improve the physical and mechanical properties of materials. The most promising is thermocycling treatment (TCT). The microstructure, substructure, and dislocation structure of metals and alloys [23; 24] undergoes a sharp change during TCT, which determined the choice and application of the TCT method for structure formation in DHA. The development of TCT regimes in each specific case has an individual character, since the change in the structural state and properties of materials during TCT depends on many factors. Therefore, it is necessary to develop those processes, the action of which leads to the achievement of the optimal structure and properties of the material.

In this work, DHA based on aluminum $Al, Al-(1,0;2,0;3,0;4,0)\%\,wt.Cu$, $Al, Al-(1,0;3,0;4,0)\%\,wt.Zn$, $Al-4,0\%\,wt.Cu-1,0\%\,Zn$ and $Al-4,0\%\,wt.Cu-6,0\%\,Zn$ were investigated. These materials, on the one hand, they are promising structural materials, and, on the other hand, their study is of scientific interest, since it is possible to combine two types of strengthening: substructural strengthening and dispersion hardening. The production of samples was carried out by means of rolling and drawing through dies. The fusion of aluminum with copper and zinc was carried out in glass-graphite crucibles under a flux. The flux was made from *NaCl* and *KCl* salts. After melting, the alloy was poured into a groove made of pure graphite. In this way, rods with a diameter of 6-7 mm were obtained, which were processed by rolling and drawing to the required diameter. To remove possible contamination of the surface of the samples they were treated chemically in *NaOH* solution. Thermocycling was carried out in the temperature range $(283\div 423)K$ under an external voltage of $(0,2\div 0,65)\sigma_{0,2}$. The rate of heating and cooling cycles was maintained in the range of $1-5\,K\cdot s^{-1}$.

IF was measured after each cycle at a frequency of $\sim 1Hz$. The amplitude of deformation of the temperature dependence of IF (TDIF) did not exceed 10^{-5}. Amplitude dependence of IF (ADIF) was studied in the range of amplitudes of shear deformation $(1\div 100)\cdot 10^{-5}$.

Microhardness studies were carried out under a load of 0.50 *N*. Holding under the load lasted 10 *s*. Processing of samples was carried out in conditions adequate for processing for measuring IF. Each microhardness value was selected as the average of 10-15 indenter injections.

3.2. Choosing a research method

To study the influence of the thermal and force field on the mechanical properties of the material, a comprehensive analysis of its elastic and inelastic characteristics was used. The main tool is the method of low-frequency internal friction with synchronous fixation of the effective torsional modulus, which was measured using an inverse torsional pendulum, in which the sample is the elastic part of the oscillating circuit. Its advantages are as follows:

– it is a non-destructive method and provides control of the state of the defective subsystem in the process of microplastic deformation;

– does not require a large amount of material;

– allows conducting research in a wide range of temperatures, amplitudes of microdeformations, magnetic field strength;

– has a high selective sensitivity to changes in the defective structure of materials, in particular the dislocation-impurity structure, which is responsible for the magneto-mechanical effects in diamagnets.

One of the features of the reverse torsional pendulum (compared to the direct or horizontal) is that the frequency of the natural oscillations of the system is determined not only by the elastic properties of the sample, but also by the stiffness of the torsion. Its presence significantly increases the mechanical *Q*-factor of the combined oscillatory system and makes it possible to carry out measurements with large losses of mechanical energy in the sample material, which, in the absence of torsion, would make the study of strongly damped oscillations impossible at all, since the process would become aperiodic.

3.3. Installation for thermocyclic processing of materials in a loaded state and measurement of internal friction

Internal friction in solid bodies is the property of solid bodies to irreversibly transform into thermal (dissipative scattering) mechanical energy, which was given to the body in the process of its deformation [4; 5; 9].

There are many experimental methods for determining the characteristics of energy dissipation in a material [28]. In the practice of materials science, the measurement of IF in the mode of free damping oscillations is carried out first of all with the help of an inverted torsional pendulum. Measurements of the value of IF are connected with the need to fix the light "bunny". In the case of visual determination, the accuracy of measurements depends on the experience of the experimenter. The task is greatly simplified with the use of photosensitive elements [29]. Determination of the logarithmic decrement of oscillations in many cases is carried out by decreasing their amplitude. To reduce the time of one measurement, it is proposed to determine the decrement by decreasing the speed of the light beam passing the equilibrium position [30]. Even more perfect is the method of measuring the time intervals of the flight of a light "bunny" between two fixed points relative to the center of equilibrium of the pendulum. For this, low-inertia photodiodes are successfully used [26; 29; 30].

Therefore, in order to study the structural state of materials by the IF method and their thermal cycling in a loaded state, a device was developed for automatic registration of the shear modulus, temperature, amplitude and time dependences of IF at low frequency $(\sim 1\text{Hz})$ based on the models described in works [26; 27; 29; 30]. In order to ensure the possibility of reliable comparison of ADIF of metals and alloys with their "stress-strain" diagrams, a modification of the relaxor (power part) was created [27; 29], which allows simultaneous measurement of IF and deformation as a function of applied mechanical stress, as well as thermocycling of samples in a loaded state.

The device (Figure 3.2) consists of the following parts (blocks). The inertial part (1) is a vacuum head with an inverted torsional pendulum, which allows measurements in the temperature range from 193 to 1150 *K*. The range of working deformation amplitudes is from 10^{-6} to 10^{-3}. Samples with a length of 50-200 mm with a round or rectangular section are used. Installation background $<10^{-4}$ IF units. The measurement error does not exceed 2-5%. It is possible to create an external magnetic field up to 40000 *A/m* (unit 4).

The power supply unit, heating and temperature regulator (2) is an electronic device for the formation of quasi-linear alternating voltage of high power [26; 29]. The heating and cooling rate ranges from $0{,}1K\,s^{-1}\left(5K/min\right)$ to $2{,}1K\,s^{-1}\left(125K/min\right)$.

The cooling unit (3) is a protective water jacket around the heating furnace, as well as cooling the test sample using air or liquefied gas blowing.

Load block (5), which serves to create an external load on the sample [29; 27]. The load is controlled by a strain gauge, which is made according to the scheme of a strain gauge bridge consisting of 4 strain gauges (Figure 3.1, a).

From the strain gauge bridge, voltage is supplied to the Topaz-3 amplifier, and from it to the KSP-4 potentiometer and a millivoltmeter or oscilloscope. The millivoltmeter is graduated in units of force. On the other hand, the force applied to the sample can be found from the resulting oscillogram, the approximate appearance of which is shown in Figure 3.1, b.

According to the oscillogram, the value of the parameter (force) at a given time is determined by the expression:

$$P_t = P_m \frac{H_p}{H_m}, \tag{3.1}$$

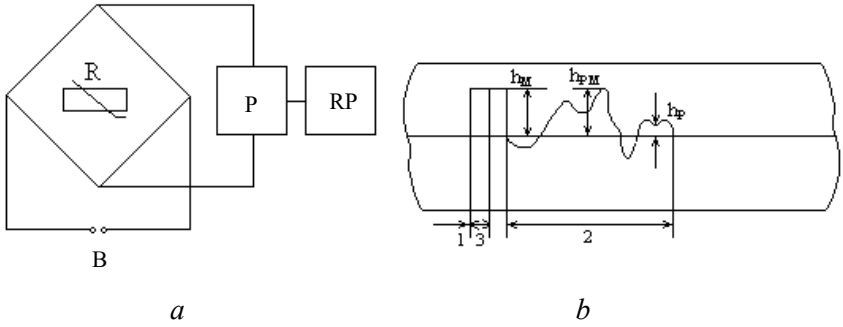

a *b*

Figure 3.1. Scheme of a strain gauge device of direct action. (a): B – current source; P – amplifier; R – tensile strength; RP – recording device and oscillogram (b): 1 – "zero" signal; 2 – working signal; 3 – scale signal

where P_m – is the scale value of the measured parameter in natural units; H_p, H_m – working and scale value of the ordinate, mm.

The deformation of the sample is controlled using a differential transformer [31]. The data of the differential transformer is fed to the amplifier, and after it is recorded by a voltmeter and potentiometer KSP-4. With the help of grading coefficients, we determine the absolute elongation and the degree of deformation. The sensitivity of the differential transformer is 1-2 %. The rate of deformation was set by the EVP-9 system, which made it possible to change the rate in the range from $0,006\,mm \cdot c^{-1}$ to $1,5\,mm \cdot c^{-1}$. The collected information is transferred to a computer, which after processing produces results in the form of tables and graphs.

The correction for sample elongation during tensile testing was calculated according to the equation [31]:

$$\Delta = \frac{0,25 \cdot l^3 \cdot F_t}{10^3 \cdot b \cdot h^3 \cdot E}, \qquad (3.2)$$

where *l, b, h* – the length, width and height of the base to which the tension supports are attached (l = 113.70 *mm*, b = 35.33 *mm*, h = 1.60 *mm*); E – modulus of elasticity (E = 200 *GPa*).

Registration block (6). Since the logarithmic decrement of free oscillations is measured, a light "bunny" was chosen as the connecting link

between the inertial and recording parts, which makes it possible to reduce the effect on the oscillating system of side forces to zero. The influence of the atmosphere is eliminated by placing the system in a vacuum [30]. This factor was taken into account when choosing the automatic pumping method. For registration, photodiodes FD-256 (photosensitive area 1,3 mm^2) were chosen. The optimal size of the light beam is 3-6 *mm*. The block diagram of the measuring part of the installation is shown in Figure 3.3.

A method of transmission and reception of light information has been developed, based on the principle of recognition of the optical signal coded by the receiver of frequency modulated light. The lighting system forms a light stream with a certain fixed parameter (frequency) to illuminate the modulated optical signal. Thus, the operation of the photodetector does not depend on the level and variations of illumination on the photosensitive element.

Optical signals of a certain fixed frequency are generated in the illumination system (IS) and fall on the relaxer mirror. The light "bunny" reflected by it passes through a photosensitive element (PE), which converts light pulses into a voltage of a certain frequency. Through the filter (F), which blocks the passage of frequencies of 50 and 100 *Hz* (for example, from lighting devices), the signal enters the input of the operational amplifier (A). The detector (D) detects an amplified signal of a fixed frequency, and the pulse forming unit (PFB) forms logical zero pulses (while protecting the system from random impulse interference), which are fed to the corresponding input of the recording device.

As a lighting system, a source of radiation of inertialess light flashes is used, the frequency of which can be adjusted. This makes it possible to easily select the frequency of light pulses to which the photodetector is set.

This design of the installation allows to simultaneously receive information through three channels: to a digital printing device or a punch at the values of the amplitude of oscillations from A_0 to A_n and the time of passage of the light beam through the constant base at the beginning of the countdown and after n oscillations; the main graph of temperature, amplitude and time dependence of IF is displayed on the graph plotter. This not only increases the informativeness and reliability of the results, but also provides an opportunity for prompt intervention by the experimenter to change the measurement mode and process the results using a computer.

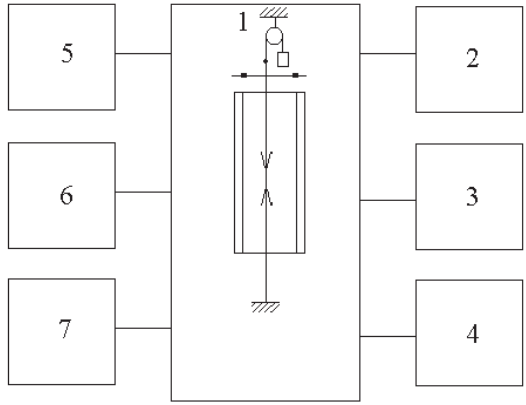

Figure 3.2. Block – diagram of the main units of the installation: 1 – inertial part; 2 – power supply unit; 3 – cooling unit; 4 – unit for creating a magnetic field; 5 – load generation unit; 6 – registration unit; 7 – Computer

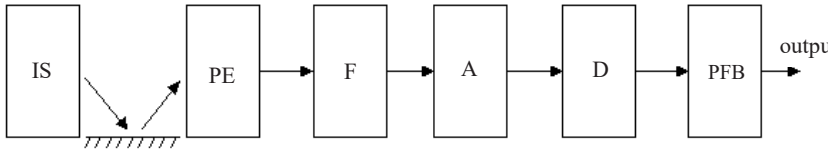

Figure 3.3. Scheme "illuminator-sensor"

In addition, the installation is designed in such a way that it is possible to carry out thermal cycling under the influence of an external force without dismantling the sample. The thermocycling process proceeds as follows. The sample is automatically heated in the oven to the selected maximum temperature. Next, the furnace is opened and simultaneously the outlet valve of the cylinder with carbon dioxide or nitrogen is opened, as a result of which the sample is rapidly cooled to 273–293 *K*. When a temperature of 273–293 *K* is reached, the outlet valve and the furnace are closed and reheating is carried out. With the help of a strain gauge, the external load on the sample is regulated.

The number of thermocycles depends on the next task of the experiment. On the last TCT cycle, when the temperature in the sample area is maximum,

the voltage from the furnace is turned off and cooling is carried out to a temperature of 273–293 *K*. At the end of the cycle, the external load is removed. After that, IF measurements are carried out, the results of which are processed on a computer.

3.4. Methodology of the research of the elastic and inelastic characteristics

Different values can be chosen as a measure of internal friction [6; 9; 28; 29; 30]. The most well-known measure of IF of an oscillating system is the value that is the inverse of its Q factor:

$$Q^{-1} = \frac{\Psi}{2\pi}, \tag{3.3}$$

where $\Psi = \frac{\Delta W}{W}$ – is the energy absorption coefficient, which can be determined according to the sweep of freely damped vibrations of the sample under study [28].

In this case, the value of Ψ will be equal to:

$$\Psi = -\int_{t}^{t+T} \frac{dW}{W}. \tag{3.4}$$

Since the value of W is proportional to the deformation amplitude $A_0^2(t)$, where $A_0(t)$ – is the envelope of the curve of free damping oscillations, we obtain:

$$\Psi = -2\int_{t}^{t+T} \frac{dA_0(t)}{A_0(t)} = 2\ln\frac{A_k}{A_{k+1}} = 2\delta, \tag{3.5}$$

where $\delta = \ln\frac{A_k}{A_{k+1}}$ – is the logarithmic decrement of attenuation.

The equality between δ and Ψ is valid for any deformation amplitudes and does not depend on the energy dissipation mechanism. Therefore, the following equation can be used to measure the IF value:

$$Q^{-1} = \frac{\delta}{\pi} = \frac{\ln\frac{A_k}{A_{k+1}}}{\pi}, \tag{3.6}$$

If we take into account that in the experiment the number of oscillations n is greater than one, then equation (3.6) can be rewritten in the form:

$$Q^{-1} = \frac{\ln \frac{A_k}{A_{k+n}}}{\pi n}. \quad (3.7)$$

Using this equation, we determined the dependence of the value of IF on the temperature and the amount of deformation. But, depending on the nature of the experiment, the amplitude interval (A_k, A_{k+n}) and the number of oscillations n in it were chosen in such a way that the envelope curve of free oscillations could be approximated by a linear function with a sufficient degree of accuracy. In some cases, special methods of measuring the Q^{-1} value were used. Having placed the photosensors at a distance l from the center of the freely falling amplitude of the light beam, the authors [56] showed the dependence of the deformation amplitude on the measurement time, i.e.:

$$l = B_1 \sin(\omega_1 t_1) exp(-\lambda t_1), l = B_2 \sin(\omega_2 t_2) exp(-\lambda t_2). \quad (3.8)$$

Since $B_1 / B_2 = A_1 / A_2$ and taking into account equalities (3.5) and (3.7), we obtain:

$$\delta = \frac{1}{n} \cdot \frac{\sin(\omega_1 t_1) exp(-\lambda t_1)}{\sin(\omega_2 t_2) exp(-\lambda t_2)}. \quad (3.9)$$

Approximating this expression, we find:

$$\delta = \frac{1}{n} \cdot \frac{\sin(\omega_1 t_n)}{\sin(\omega t_1)}. \quad (3.10)$$

Using expression (3.10) and using highly sensitive equipment, it is possible to determine the decrement of oscillations of the material under study with high accuracy [30]. In work [29], the logarithmic decrement was calculated by determining the speed of passage of the light beam through the equilibrium position of the system when the oscillations are damped, i.e.:

$$\delta = \frac{1}{n} \cdot \ln\left(\frac{v_0}{v_n}\right), \quad (3.11)$$

where v_0 – is the speed of light passing through the constant base at the beginning of the countdown; v_n – speed of passage of a light beam of a constant base after n oscillations.

If t_0 – is the time of passage of a light beam through a constant base at the beginning of the countdown, and t_n – is the time of passage of a beam

through the same base after *n* oscillations, then averaging the speed over this distance gives [29]:

$$\delta = \frac{1}{n} \cdot \ln\left(\frac{t_0}{t_n}\right). \tag{3.12}$$

The last expression makes it possible to significantly increase the accuracy of determination of IF. With the help of formulas (3.7) and (3.12), the dependence of the value of IF on the temperature T and the amount of deformation γ was determined.

3.5. Methods of processing experimental data of temperature and ampli-tude dependences of the internal friction

3.5.1. Analysis of relaxation spectra of mechanical spectroscopy

A relatively weak low-temperature background at $T < (0{,}5 - 0{,}6)T_{pl}$, a high and sharply increasing high-temperature background with increasing temperature, and two types of maxima: relaxation and hysteresis maxima are observed at the TDIF. The former have a Debye shape [28] and shift with increasing frequency of oscillations *f* towards higher temperatures:

$$Q^{-1} = \frac{\Delta}{\sqrt{1+\Delta}} \cdot \frac{\omega\tau}{1+(\omega\tau)^2}, \tag{3.13}$$

where $\Delta = (M_n - M_r)/M_n$ – is the degree of relaxation, which characterizes the intensity of the relaxation process; M_n, M_r – non-relaxation and relaxation modulus of elasticity, respectively; ω – is the frequency. The relaxation time τ, according to the Arrhenius law, depends on the temperature:

$$\tau = \tau_0 \exp\left(\frac{H}{RT}\right), \tag{3.14}$$

where τ_0 – is the oscillation time of atoms, which does not depend on temperature; *H* – enthalpy (energy) of activation of the relaxation process; *T* – temperature; *R* – universal gas table.

If IF is caused by a relaxation process, the relaxation time of which τ_r is such that

$$\tau_r > \frac{\sqrt{3}}{12\pi^2} T_0 \approx 1{,}46 \cdot 10^{-2} T_0, \tag{3.15}$$

where T_0 – is the period of natural oscillations, then IF is determined by the ratio:

$$Q^{-1} = \frac{2\sqrt{3}}{3} th\theta + \frac{\left(\omega_0^2 - \frac{ch\theta}{3\tau_r^2}\right)^{-1/2}}{3\tau_r}. \quad (3.16)$$

The value of θ is determined from the equation:

$$sh3\theta = \frac{\left(\frac{1}{3\tau_r}\right)^3 + \frac{\omega_0^2}{2\tau_r}\left(\frac{E_r}{E_n} - \frac{1}{3}\right)}{\left(\frac{\omega_0^2}{3} - \frac{1}{9\tau_r^2}\right)^{3/2}}. \quad (3.17)$$

Solving equations (2.16) and (2.17) on a computer with respect to τ_r, we obtain the relaxation time of the process that determines this effect and the activation energy of the process *H*

The enthalpy (energy) of activation *H* of the relaxation process, if it is connected with the thermally activated movement of atoms to a distance of the atomic order, is determined from the Werth-Marx formula [33]:

$$H = RT_m \ln\frac{kT_m}{h\omega} + T_m\Delta S, \quad (3.18)$$

where h – is Planck's constant; ΔS – activation entropy $(10-12\,J/mol)$. The entropy term can be neglected, which will give an error of $\frac{\Delta H}{H} = 2-5\%$. But one can always expect the appearance of a sufficiently large non-excluded systematic error due to differences in the relaxation process from the ideal Debye model.

If you change the frequency of oscillations of the sample from f_1 to f_2, the relaxation maximum Q_m^{-1} will shift along the temperature scale and the value of H will be determined by the formula:

$$H = R\frac{T_{m1}T_{m2}}{T_{m1} - T_{m2}} \ln\frac{f_2}{f_1}. \quad (3.19)$$

To accurately calculate the enthalpy of activation of the relaxation spectrum, it is necessary to replace the frequency of oscillations of the sample by several orders of magnitude, since the shift of the IF peak by 20-40°C gives a relative error in the calculation of*H* of about 20%. It is

possible to increase the accuracy of measuring the temperature shift $T_{m2} - T_{m1}$ by plotting the shape of the maximum on the curves of TDIF in hyperbolic coordinates followed by approximating the resulting graph with a linear regression equation. Thus, the value H of the relaxation process can be determined based on the analysis of the shape of the peak on the temperature dependence of the internal friction (TDIF) by graphical or analytical methods.

In addition, if you use the measurement data of TDIF, curves in the region of the maximum in the hyperbolic coordinate system are constructed with the help of a computer [34]:

$$arsec\,h\left(Q_p^{-1} / Q_m^{-1}\right) = f\left(1/T\right). \tag{3.20}$$

That is, the computer reconstructs the relaxation maximum in a straight line and calculates the temperature T_m and the activation enthalpy H, since the point of intersection of the line with the abscissa axis gives the temperature T_m, and the slope of the line allows you to determine the enthalpy of the process. If there are several partial maxima of Q_m^{-1} on the temperature axis, it is possible to use a computer to highlight the corresponding branches for each of them on the "hyperbolic grid" [28] (Figure 3.4).

Figure 3.4 shows the resulting curves of the temperature dependence of IF of aluminum, after the substructure formed in it, on a hyperbolic grid. Dependence (2.20) consists of three rectilinear sections (Figure 3.4, a), which are connected by a transition region. From the constructed graph, the temperature value is determined with an accuracy of 2-3 degrees.

According to the location of the transition region on the curves of TDIF in the hyperbolic grid and the mutual placement of rectilinear sections on them, it is possible to say that the partial maxima of IF are equal or different in magnitude. When the heights of the maxima are different, the smaller rectilinear section corresponds to the maximum of a smaller height and the transition region shifts to its side. If the heights of the maxima are equal, then the transition region will be located in the place of the hyperbolic grid where $\frac{Q_p^{-1}}{Q_m^{-1}} = 1$.

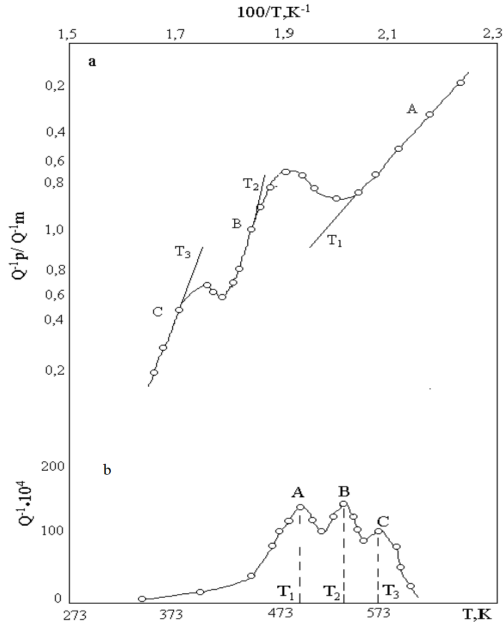

Figure 3.4. Temperature dependence of the internal friction of substructurally strengthened aluminum in the hyperbolic coordinate system (a) and the $Q^{-1} = f(T)$ coordinate system (b) [34]

3.5.2. Processing of the results of the amplitude dependence of internal friction. Critical strain amplitudes and dislocation structure parameters

Amplitude-dependent internal friction (ADIF) allows not only to evaluate the entire set of characteristics of the dislocation structure, but also to follow their development under the influence of temperature-time and force factors. Among various models of ADIF, the Koehler-Granato-Lucke model is the most universal [5; 6].

The Koehler-Granato-Lucke theory made it possible to explain energy dissipation with the help of dislocations, which are considered in it as oscillating strings. Analytical substantiation of the theory of ADIF and its modifications is given in [28].

In the first region of the amplitude-independent IF $(\gamma < \gamma_{cr.1})$, the main contribution to damping at small deformations is made by the oscillations of dislocation segments (L_s), which are fixed by impurity atoms or vacancies. In this case, the expression for δ_1 can be written in the form:

$$\delta_1 = \frac{120\Omega B_0 \omega \Lambda L^4}{\pi^4 C}, \tag{3.21}$$

where B_0 – is a constant attenuation; C – is the force per unit length of the dislocation, which is caused by the tension of the bent dislocation.

In the second region, which corresponds to deformations $\gamma_{cr.1} < \gamma < \gamma_{cr.2}$, dislocations detach from impurity atoms and they remain fixed only at the nodes of the dislocation lattice L_n. Dissipation of mechanical energy in materials is described by the formula:

$$\delta_2 = \frac{C_1}{\gamma} \cdot exp\left(-\frac{C_2}{\gamma}\right), \tag{3.22}$$

where C_1 and C_2 – are the coefficients that are determined from the ADIF data in Granato-Lucke coordinates. The constant C_1 is related to the density of dislocations Λ or the ratio ρ:

$$C_1 = A_1 \Lambda L_n^3 / L_s^2, \tag{3.23}$$

and the constant C_2 is determined by the length of the dislocation segment:

$$C_2 = k\eta a / L_s, \tag{3.24}$$

where η – is the Cottrell mismatch parameter $(\eta = (D_a - D_b)/D_a$, where D_a – is the diameter of the matrix atom; D_b – is the diameter of the impurity atom); $a = b$ – Burgers vector; $k \sim 0,2$.

The second critical deformation amplitude $\gamma_{cr.2}$, corresponds to the stress that causes the generation of dislocations by sources of length L_n according to the Frank-Reed mechanism [28]. From this amplitude, the increase of the IF background begins. There is a relationship between the values $\gamma_{cr.2}$, L_n (dislocation length between strong anchoring points) and the Burgers vector b:

$$L_n = b / \gamma_{cr.2}. \tag{3.25}$$

Equations (3.23) – (3.27) make it possible to find the parameters of the dislocation structure L_s, L_n and Λ. In addition, the ADIF method allows you to determine the binding energy of the dislocation H_d with the blocking atom by the value $\gamma_{cr.1}$ and the defect of the module $\Delta M / M$:

$$\gamma_{cr.1} = \frac{H_d c_d}{Mb^3}, \tag{3.26}$$

$$\frac{\Delta M}{M} = \frac{6\Omega L^2}{\pi^2}, \tag{3.27}$$

where c_d – is the concentration of impurity atoms on dislocations $\left(c_d = L_n / L_s\right)$; Ω – is the orientation factor; L – is the effective length of dislocations $\left(1/L = 1/L_s + 1/L_n\right)$.

At deformation amplitudes $\gamma > \gamma_{cr.2}$, the dissipation of mechanical energy is caused by plastic deformation in local volumes. The value of δ_3 in this case can be estimated by the formula:

$$\delta_3 = \frac{\omega\left(n_1 b\right)^2 \Lambda_1 d^2 B_0 \gamma_0^{m-2}}{q\gamma_T^m}, \tag{3.28}$$

where n_1 – is the number of loops generated by one source; Λ_1 – volume density of active dislocations; d – displacement area per oscillation cycle; q – distance between sliding planes; m and B are constants that depend on the dispersion of the stress distribution curve across grains; γ_T – is the deformation that corresponds to the yield strength of the hardening grains; γ_0 – current amplitude of periodic deformation. But equation (3.10) has not yet been fully experimentally verified and cannot be used for practical evaluation of the parameters of the dislocation structure of a metal by the ADIF method at the stage of microfluidity.

3.5.3. Determination of damping and substructural characteristics based on the results of experimental curves of ADIF

IF was determined by the formula (3.7), and the deformation amplitude by the formula:

$$\gamma = d\left(A_0 + A_n\right) / \left(4lZ\right), \tag{3.29}$$

where d – is the sample diameter; l – is the length of the sample; Z – the length of the optical lever; A_0, A_n – is the initial and final amplitude, respectively.

The critical deformation amplitudes shift towards smaller amplitudes with increasing temperature. This indicates that an increase in temperature gives dislocations energy to break away from stoppers of low power

(impurity atoms, vacancies) $\gamma_{cr.1}$, as well as from stoppers of high power (dispersed al-locations, accumulation of impurity atoms, etc.) $\gamma_{cr.2}$. In addition, when the deformation amplitude increases and decreases, the hysteresis on the ADIF curves is Q^{-1}. These characteristics make it possible to esti-mate the dislocation characteristics of the material structure (see equations 3.23-3.27).

Thus, the first critical deformation amplitude $\gamma_{cr.1}$ can be determined by the beginning of the amplitude dependence of IF and the beginning of the amplitude dependence of the $\Delta M / M$ module defect, and the second – by a sharp break in the ADIF, an increase in the background of the ADIF Q_f^{-1} and a sharp increase in the module defect.

The defect of the modulus of elasticity from the experiment is determined by the ratio:

$$\frac{\Delta M}{M} = \frac{\Delta f^2}{f_0^2} = \left(f_0^2 - f^2 \right) / f_0^2, \qquad (3.30)$$

where f_0 – is the frequency of oscillations at the initial deformation amplitude; f – is the frequency of oscillations at the current deformation amplitude.

The next characteristic of ADIF is the slope of the Q^{-1} curve to the abscissa axis, which is determined by the value of $tg\alpha$. This value characterizes the intensity of detachment of dislocations from stoppers of different strength.

$tg\alpha_1 = \dfrac{Q^{-1}}{\Delta\gamma}$ – characterizes the intensity of detachment of dislocations from weak anchoring points (impurity atoms), an increase in L_c.

$tg\alpha_2 = \dfrac{Q^{-1}}{\Delta\gamma}$ – characterizes the intensity of detachment of dislocations from strong anchoring points (dispersed phases, clusters), generation of dislocations by the Frank-Reed mechanism. The value of $tg\alpha$ of ADIF depends on the number of anchoring points, the strength of the connection and the width of the dislocation. A decrease in $tg\alpha$ indicates an increase in the degree of anchoring of dislocations. The growth of the ADIF background after the second critical is caused by an increase in the density of dislocations that are generated in the process of microplastic deformation.

Coefficients C_1 and C_2 can be determined from the ADIF graph constructed in Granato-Lyukke (GL) coordinates $ln(\gamma Q\pi)-\gamma^{-1}$.

Calculations of the parameters of the dislocation structure, made on the basis of the GL theory, correspond to the results of the experiment for deformations $\gamma_{cr.1} < \gamma < \gamma_{cr.2}$. But in this case, C_1 and C_2 directly describe the experimental dependence only in a narrow region of the spectrum of the amplitude dependence of IF, therefore, based on the Granato-Lucke theory, the authors [35] propose a description of ADIF in all areas by the method of regression analysis. The experimental dependence is well described by the formula:

$$\delta = \sum_{i=1}^{\Lambda} \delta_i \tag{3.31}$$

where δ_i is calculated on the basis of the GL theory [6] according to formulas (3.22, 3.31). Using this method, a system of linear equations of the form is solved:

$$\begin{cases} \dfrac{\partial \delta}{\partial (\ln C_1)} = \sum\limits_{i=1}^{\Lambda} \left[\ln \delta_i - \left(\ln C_1 - \ln \gamma_i - \dfrac{C_2}{\gamma_i} \right) \right]^2 = 0 \\ \dfrac{\partial \delta}{\partial C_2} = \sum\limits_{i=1}^{\Lambda} \left[\ln \delta_i - \left(\ln C_1 - \ln \gamma_i - \dfrac{C_2}{\gamma_i} \right) \right]^2 = 0 \end{cases}, \tag{3.32}$$

the solution of which is the equation:

$$C_2 = \frac{\Lambda \sum_{i=1}^{\Lambda} \left[\left(\ln \delta_i + \ln \gamma_i \right) \frac{1}{\gamma_i} \right] - \sum_{i=1}^{\Lambda} \left[\ln \delta_i + \ln \gamma_i \right] \sum_{i=1}^{\Lambda} \frac{1}{\gamma_i}}{\left(\sum_{i=1}^{\Lambda} \frac{1}{\gamma_i} \right)^2 - \Lambda \sum_{i=1}^{\Lambda} \frac{1}{\gamma_i^2}},$$

$$C_1 = exp\left[\frac{1}{\Lambda} \left(\sum_{i=1}^{\Lambda} \left(\ln \delta_i + \ln \gamma_i \right) + C_2 \sum_{i=1}^{\Lambda} \frac{1}{\gamma_i} \right) \right]. \tag{3.33}$$

Calculation of constants C_1 and C_2, according to expressions (3.32, 3.33), is best done on a computer. This allows you to avoid random experimental values by smoothing the experimental data using the parabola method before starting the calculations, and to avoid the cumbersome

calculations. Thus, according to expressions (3.32, 3.33) and the theory of GL, we have the opportunity to calculate the parameters L_s and L_n between the weak and strong points of anchorages, the density of dislocations Λ, the concentration of point defects on dislocations c_d, as well as the energy of the dislocation connection with atoms and the defect modulus.

In Table 3.1. compared the results of calculations for $Al - wt.4\%Cu$ alloy by methods [6] and [35]. Moreover, the latter correlate well with experimental data. The difference between them does not exceed 3-5%.

Table 3.1

The parameters of the dislocation structure, calculated by methods [6] and [35]*

N	$L_n \cdot 10^6$, *m*		$L_s \cdot 10^8$, *m*			$\Lambda \cdot 10^{-12}$, m^2			C_d	
TCT	**A, B**	***GL***	**A**	**B**	***GL***	**A**	**B**	***GL***	**A**	***GL***
0	2,3	5,2	11	1,3	10,7	55	7,9	39,3	20	28
5	2,3	2,4	12	1,4	12,6	40	4,7	32,6	19	19
10	1,9	1,9	11	1,2	11,2	55	9,5	47,0	18	17
25	1,2	2,0	8	0,87	7,5	60	19,0	39,0	15	27
50	1,7	0,95	9,3	0,9	6,5	62	14,0	63,0	19	15

Notes*: 1. *A* ($\gamma_{cr.1} < \gamma < \gamma_{cr.2}$), *B* ($\gamma > \gamma_{cr.2}$) – the calculation of dislocation structure parameters was carried out according to the method [35]; 2. *GL* ($\gamma_{cr.1} < \gamma < \gamma_{cr.2}$), – according to the method [6]; TCT – thermocycling treatment

At rather small values of deformation amplitudes, microplasticity is manifested, which is caused by the movement of dislocations in the field of alternating stresses. In this regard, the phenomenon of IF is the most informative [28; 36]: with the growth of the deformation amplitude, more and more dislocation sources are included in the energy dissipation in the material, the contribution of which to the total energy absorption of mechanical vibrations is different. Dissipated energy per oscillation cycle in a unit volume ΔW (or internal friction Q^{-1}) can be defined as:

$$\Delta W = \sum_{i=1}^{n} \Delta W_i, \quad Q^{-1} = \sum_{i=1}^{n} Q_i^{-1}, \tag{3.34}$$

where $\Delta W_i\,(Q_i^{-1})$ – is the dissipated energy associated with the *i*-th mechanism, *n* – is the total number of sources (mechanisms).

If we give a certain meaning to each $\Delta W_i\,(Q_i^{-1})$ and critical deformation amplitudes at which a change in the dislocation mechanisms of energy

dissipation is possible, then the generalized dependence of $Q^{-1}(\mu)$ for many metals and alloys can be written in the form

$$Q^{-1}(\varepsilon)=\varphi_1(\varepsilon)+\frac{\varphi_2(\varepsilon)}{\varepsilon-\varepsilon_{cr.1}}\cdot exp\left[\frac{C_2}{\varepsilon-\varepsilon_{cr.1}}\right]+\varphi_3(\varepsilon)\cdot\frac{(\varepsilon-\varepsilon_{cr.1})1^{m-2}}{\varepsilon_{cr.2}^{m}}, \quad (3.35)$$

where – $\varphi_1,\varphi_2,\varphi_3$ can be determined by calculation, and the coefficients C_2, m and the critical deformation amplitudes $\varepsilon_{cr.1}$, $\varepsilon_{cr.2}$ and $\varepsilon_{cr.3}\cdot(\gamma_{cr.3})$ – experimentally.

At amplitudes $\gamma<\gamma_{cr.1}$, IF practically does not depend on the deformation amplitude. In the range of deformation amplitudes from $\gamma_{cr.1}$ to $\gamma_{cr.2}$. IF is reversible when the load is removed (dislocation hysteresis) and depends little on the amplitude of the deformation. This load area is characterized by closed-type hysteresis loops and the appearance of a defect in the modulus of elasticity (EMD) $\Delta M/M$. At $\gamma>\gamma_{cr.2}$, there is an area of irreversible changes in the background of IF and ME after removal of the load, which are associated with plastic deformation in individual microvolumes, and the formation of open-type loops (plastic hysteresis.

When $\gamma=\gamma_{cr.3}$ and more, the deformation takes on a macroscopic character. That is, at such amplitudes, the cyclic load factors and, above all, the frequency and duration of the load during measurements of ADIF EMD are manifested to the greatest extent. The nature of the dependences of $Q^{-1}(\gamma)$ and $\Delta M/M$ in this area, which are related to microplastic deformation, and their parameters can differ greatly for different materials and those conditions of amplitudecyclic influence. The second critical amplitudes of deformation can also be highlighted on the ADIF. Which are related to specific orientational, substructural and structural features of the structure of alloys. The critical deformation amplitudes $\gamma_{cr.1}$, $\gamma_{cr.2}$ and $\gamma_{cr.3}$ are the most informative for the analysis of the damageability of structural metal materials, and the stresses corresponding to these critical amplitudes of deformations, by their definition, are closest to the concepts of cyclic elastic limits (σ_{el}), micro- and macrofluidity (σ_m, σ_R) [28].

Thus, the general regularity of the effect of the frequency factor on the ADIF of the EMD of metals is quite clear – as the deformation amplitude increases, its role increases. The contribution of frequency-cyclic influence is most fully manifested in the field of development of micro-

and macroplasticity. During high-frequency tests, the last, high-amplitude stage of ADIF and EMD measurements is characterized by their temporal instability and possible gradual destruction [28; 37].

3.6. Experimental error

The use of the IF method to study the defective structure of matter makes it possible to more fully understand the processes taking place in it. But most of the results obtained by this method today are of a qualitative nature. This state of affairs is explained by the fact that the obtained inelastic energy dissipation spectra do not have an unambiguous interpretation. This especially applies to the phenomena observed during the study of metastable structures, when the mobility of defective formations is possible. In such cases, the mathematical treatment of the experiment requires special care.

If the obtained dependences of IF on external factors are of a known nature, that is, some hypothesis can be applied to them, then the method of least squares is used when calculating coefficients that include structural parameters. But in many cases the hypothesis of behavior is unknown. Then it is necessary to conduct an analysis of the accuracy of each measurement of the IF value in the experiment being conducted.

The main goal in the development of installations for IF research is to achieve the minimum level of hardware losses in the system ΔQ_y^{-1}. The latter are caused by energy losses in the material of the structural elements, mechanical friction in the sample clamps, and friction of moving systems with the environment [29; 38], i.e.:

$$\Delta Q_y^{-1} \approx \Delta Q_{cl.}^{-1} + \Delta Q_{env.}^{-1} + \Delta Q_{c.m.}^{-1}, \tag{3.36}$$

where $\Delta Q_{cl.}^{-1}$ – losses in clamps; $\Delta Q_{env.}^{-1}$ – losses due to friction with the environment; $\Delta Q_{c.m.}^{-1}$ – losses in the construction material.

That is, the error of the method consists of errors introduced by the setting ΔQ_y^{-1} and the measurement method itself ΔQ_m^{-1}.

To reduce the background losses of energy dissipation in the structure and find optimal conditions for its operation, we use the method of mathematical planning [23; 39]. As an optimization parameter, the authors [29; 40] chose the IF background at 20°C (293 *K*). The influence of the following factors on the IF level was studied:

1) x_1 – microhardness ratio of clamp and sample;
2) x_2 – is the ratio of the stiffness of the rod to the stiffness of the sample ($k = (\pi d 4G) / (32L)$, G – shear modulus, d – diameter, L – length);
3) x_3 – the ratio of thread stiffness to sample stiffness.

For all factors, the zero level and variation intervals were chosen based on a priori data.

As a result of the texture experiment, the coefficients of the regression equation were calculated. The equation obtained by the authors [29; 40] has the form:

$$y = 9,22 + 1,11x_1 - 0,38x_2 + 0,62x_3 - 0,41x_2x_3. \qquad (3.37)$$

On the basis of the obtained mathematical model of the process, nomograms (Figure 3.5) were built, which can be used to determine the design parameters of the device. So, if you know the microhardness of the sample and calculate its stiffness, then the microhardness and stiffness of the rod are determined by the nomogram. Hardware losses will be minimal. For a torsional pendulum, it is recommended to choose such a system of clamps so that the ratio [28; 29; 40] is fulfilled: $(k_r / k_s) > 100$.

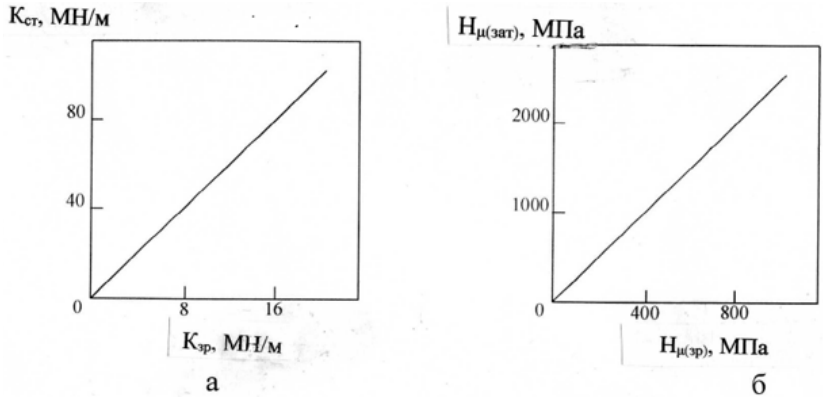

Figure 3.5. Dependence of stiffness (a) and microhardness (b) of the rod and clamps on the stiffness and microhardness of the sample for the case of minimal background losses

In addition, the source of significant systematic errors can be aerodynamic

losses, which are a function of the density of the medium and the shape of the parts of the moving system. According to the calculations made in [38], aerodynamic losses in systems of the torsional pendulum type are:

$$\delta_a = \frac{8\pi\beta\rho SR^3\varphi_0}{3k_s T^2}, \tag{3.38}$$

where β – is the drag coefficient, which at low speeds is a function of the Reynolds number; A – is the density of the surrounding medium; S – is the cross-section of the rod, which is normal to the direction of the speed of its movement; R – is half the length of the inertia bar; φ_0 – is the maximum twisting angle; k_s – stiffness of the sample; T – is the oscillation period.

Calculations showed that these losses decrease with increasing oscillation frequency and increase in proportion to the deformation amplitude. The most effective reduction of aerodynamic losses is achieved when measuring IF in a vacuum and decreases to zero at a residual pressure of 1 *Pa*.

An error occurs when measuring ADIF, which is caused by a change in temperature in the process of research. This source of additional error is most significant in the region of the maximum and high-temperature branch [28; 38]:

$$\frac{\Delta Q^{-1}}{Q^{-1}} = \frac{\left(0,4\,H\Delta T\right)}{\left(RT^2 q^{-1}\right)}, \tag{3.39}$$

where $q^{-1} = Q^{-1} / Q_m^{-1}$; Q^{-1} and Q_m^{-1} – IF at temperature T and T_m, respectively; ΔT – is the absolute error at the specified temperature T_m; H – enthalpy energy; R – universal gas table.

At an oscillation frequency of $1\,Hz$: $\frac{\Delta Q^{-1}}{Q^{-1}} = 14,3\frac{(\Delta T / T)}{q^{-1}}$ (for Snook's carbon peak, the error is about 5%). The maximum error in the area of the wax-temperature background of the IF and the rising branch reaches 10-15%.

It is known [28; 38] that in the absence of systematic errors and gross errors, the error in the determined IF can be reduced to 3-5%. It is proposed to further increase the accuracy of attenuation measurements by using automatic and semi-automatic relaxers [27–30].

The study of metastable structures has the peculiarity that it is not always possible to carry out a repeated measurement. Therefore, the experimental error should be determined by one measurement. In our case, we will use the equation [41] to determine the error:

$$\delta Q^{-1} = \left[\left(\delta A_n / A_n \right)^2 + \left(\left(A_n - A_0 \right) / n A_0 \right)^2 \right]^{1/2} / \pi n \qquad (3.40)$$

Then the relative error of the IF value can be calculated using the formula:

$$\varepsilon = \left[\left(\delta A_n / A_n \right)^2 + \left(\left(A_n - A_0 \right) / n A_0 \right)^2 \right]^{1/2} / \left(\ln A_n / A_0 \right) \qquad (3.41)$$

At fixed values of A_n, δA_n, and n, there are such values of A_0 at which ε is minimal. The dependence of the A_n / A_0 ratio with increasing A_n passes through a minimum at $A_n \approx$ 15-20 *mm*. Therefore, the amount of error in the determination of IF depends on the structural state of the material, which is expressed by the degree of damping (the number of oscillations) and is mixed with the growth of A_n.

As the number of oscillations increases, the value of the relative error decreases and asymptotically approaches 2%. An increase in the clarity of the determined amplitudes by a whole order (from δA_n = 0,2 *mm;* 2 – δA_n = 0,02 *mm*) does not cause a significant increase in the accuracy of determining the IF.

Thus, it can be seen that there are certain values of A_n, A_0 and n at which the error has the smallest value. Note also that these values correlate with the degree of metastability of the defective structure of the substance.

Therefore, when measuring IF in metastable structures, it is necessary to pre-calculate the measurement intervals in order to minimize the error.

3.7. Methodology for determining microhardness.
3.7.1. PMT-3 device

The PMT-3 device is used to determine the microhardness of materials by pressing the indenter under a load of 5 to 200*G*. In the device, the indenter is a diamond pyramid with a square base and an angle at the top between the faces of 136°. To determine the microhardness, the length of the diagonal of the imprint is measured and this value is calculated as a fraction of the division of the applied load by the surface area of the resulting imprint.

To make an impression, first of all, the researched material is placed on a table and a place for making an impression is selected under a microscope. After that, the object is moved so that the selected place on its surface falls under the point of the diamond pyramid. This is achieved by rotating the table by 180° around its central axis from stop to stop, which limit the

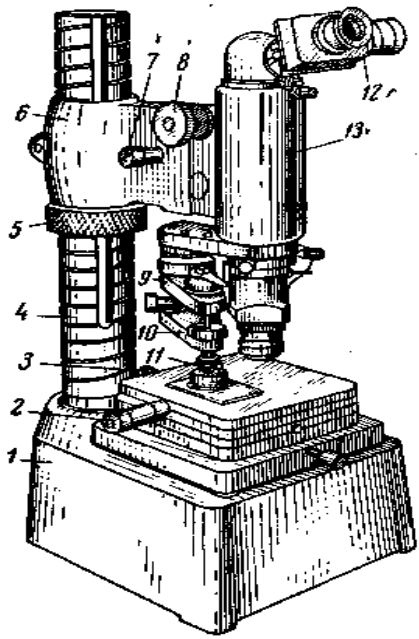

Figure 3.6. PMT-3 device: 1 – bed; 2 and 3 – table screws; 4 – rack; 5 – ring nut; 6 – bracket; 7 – microfeed mechanism; 8 – macro-feed mechanism; 9 and 10 – loading mechanism brackets; 11 – indenter (diamond pyramid); 12 – ocular micrometer; 13 – tube

rotation. In addition, the table has two translational movements of the upper part with the help of micrometric screws (2, 3).

After the researched material is placed under the indenter, pressing is carried out. Under the action of the load, as a result of the half-rotation of the arrester, the rod is lowered until the diamond pyramid collides with the object under study and, under the action of the same load, is pressed into it. To raise the rod to the previous position, the handle of the arrester is moved back.

Then the table with the object is brought to its original position and the length of the diagonal is measured under a microscope.

The size of the diagonal of the impression is determined as the product of the price of dividing the scale of the eyepiece drum by the difference of readings on the scale of the eyepiece drum when moving the intersection of lines from one corner of the impression to the opposite.

Measurements with an ocular micrometer on the PMT-3 device can be carried out with an accuracy of ±0,5 scale divisions or taking into account the magnification scale with an accuracy of up to 0,15 μm.

3.7.2. Adjustment and tare of the device

Taking into account the very high requirements for the accuracy of combining the optical axis of the microscope with the axis of the load when turning the stage, the PMT-3 device provides a special centering device that allows you to move the lens (together with the illuminator) within small limits in the horizontal plane, i.e. in directions perpendicular to to both combined axes.

To center the device, set the crosshairs of the screw eyepiece micrometer so that it is exactly in the center of the field of view of the microscope. The line in the eyepiece should be against the number 4 of the fixed scale, and zero – on the drum scale exactly against any line.

Next, we move the stage with the help of micrometric screws and bring the place chosen for the study under the intersection of threads and conduct the test. However, due to the fact that the device is not centered, the print came out away from the intersection and the intended test location. Next, we move the lens with the help of the centering screws until the intersection of the threads coincides with the center of the print a. In the future, we move the table so that the intersection again falls on the place where the impression needs to be made. The newly made impression is already found exactly in the right place.

Sometimes this operation has to be repeated several times to achieve accurate centering. Centering will be quite sufficient if the prints are located with a deviation from the overlap of the threads no more than 0,5–2,0 μm.

The loading mechanism is calibrated with a NaCl salt crystal, because when measuring the microhardness in any planes, it gives a constant value within the narrow limits of 20–22 kG/mm^2. It is also important that the microhardness of the salt remains almost constant when the load changes.

After finishing the tare of the device, the position of the load mechanism is fixed with the handle of the stopper and checked periodically.

In the PMT-3 device, special weights in the form of washers with a cutout, weighing 5, 10, 20, 50, 100, and 200 G are used for loading. When measuring, the weights are placed on the platform provided for this purpose in the space between the flat springs that support stem Permissible deviations in the magnitude of the load – for loads up to 10G no more than ±0,1%, for loads greater than 10G no more than ±1%. The error in the

magnitude of the load, which is caused by the effect of the elasticity of the spring plates themselves during pressing, is small (for example, with a print with a diagonal of 140 μ*m*, it is about 0,3*G*).

3.7.3. Measurement of the diagonal of the imprint and determination of the value of microhardness

First of all, it is important to set the eyepiece-micrometer and the impression of the diamond pyramid in such a position that when the eyepiece drum is rotated, the crosshairs move strictly along one of the diagonals of the impression.

The diagonal of the print can be measured in several ways. In our opinion, the following technique is the most convenient, which is applicable when using an ocular micrometer AM9-2 (or AM9-1).

With the help of micrometric screws of the coordinate movement of the stage, the impression is brought to the left side of the intersection of threads. Then the threads are brought with a drum to the corner of the impression. This operation should always be carried out in the same way – for example, from right to left, so that the threads always remain to the right of the contour of the impression and thereby eliminate the influence of the gaps of the screw of the counting mechanism of the eyepiece micrometer. This makes it easier to count on the scales, because first the ends of the thread are brought (from right to left) to the right corner of the print and the readings are read on the scales, then the same end of the thread is brought to the left corner of the print and the values are also read on the scales from right to left. Next, the difference of both values (*N*) is found, and the obtained result is multiplied by the price of the scale division in microns (*C*) and the length of the diagonal in microns is obtained:

$$d = CN \tag{3.42}$$

When using an epilens of aperture $A = 0{,}65$, the scale division val-ue of the indenter-micrometer drum is $C \approx 0{,}3$ μ*m*.

When studying microhardness, the numerical value of the measurement result is the fraction of the load $P(kG)$ divided by the lateral surface F of the impression (mm^2), provided that the angles in the impression are the same as in the pyramid itself:

$$H_{\mu} = P / F = (2P \sin \alpha / 2) / d^2, \tag{3.43}$$

where α – is the angle at the top of the diamond pyramid (136°, or 2,47 rads).

If P is expressed in grams, a d – in micrometers, then the formula for calculating microhardness will take the form:

$$H_{\mu} = 1854P / d^2, kG / mm^2 \quad (3.44)$$

Under the same conditions, the formula can be used to calculate the indentation depth on completely plastic materials that do not have elastic recovery

$$t = \frac{d}{2\sqrt{2}\, tg\frac{\alpha}{2}}, \quad (3.45)$$

which for α=136° takes the form:

$$t \approx \frac{d}{7}. \quad (3.46)$$

3.7.4. Estimation of the microhardness measurement error

The main error in the measurement of microhardness is the error associated with measuring the diagonal of the prints. The following causes contribute to this: deformation of the edges of the print, uneven illumination, parallax, the method of threading the threads of the screw eyepiece-microscope, inaccuracy of the loading mechanism tare (systematic errors), focus settings, threading of the eyepiece-micrometer, as well as the inaccuracy of taking the results on the drum of the screw eyepiece-micrometers (random errors). All the listed factors have a complex effect on the error in determining the size of the diagonal of the print.

The use of a pyramid with a square base is due to the fact that the conditions of deformation in the planes perpendicular to the direction of movement of the indenter are different in different directions and are repeated for the corresponding directions of the symmetrical sections of the section. Therefore, the increase or decrease of the cut surface near the corner of the impression will be less than in the middle of its sides. Thus, the sides can be either convex or concave. Distortion of the shape of the sides of the prints in the specified microhardness can lead to an error of 5-10%.

You can increase the accuracy of the measurement if you increase the contrast of the image and increase the power of the optical system. The best way to do this is to increase the numerical aperture, since the use of

large aperture values helps to reduce the amount of permissible error when measuring the diagonal of the print. The usual value of the error is from 0,5 to 1,0 μ*m*, which for ordinary prints is on average from 1 to 5%.

The random error can be additionally increased as a result of parallax of the image of the eyepiece-micrometer threads and the image of the research object itself. To avoid this, it is necessary to carefully set the eyepiece (lens) on a clear image of the threads, and the microscope tube on a clear image of the print. It is necessary to determine the price of the division of the indenter-microscope with the same installation, then the influence of parallax will be the smallest.

Another possible error is related to the inaccurate combination of the thread of the eyepiece with the contour of the impression, which should be considered the beginning or end of the diagonal.

The magnitude of this error on the PMT-3 device can reach up to 0,5 μ*m* for individual researchers, and for the same researcher, the error usually occurs in the same direction, that is, either in the direction of increase or in the direction of decrease, that's why it belongs to systematic errors.

The random error that occurs when measuring the diagonal of the impression is due to the fact that the reading on the drum of the screw eyepiece-micrometer is carried out with an accuracy of ±0,25 divisions. This accuracy corresponds to an accuracy of ±0,07 μ*m* when working with a magnification of 500 times and decreases when determining the average value from several measurements.

Other possible measurement errors are also associated with the screw eyepiece micrometer. So, for example, it is necessary to take into account the back-lash ("backlash") of the screw, the inaccuracy and unevenness of the screw pitch and measure the diagonal of the impression by uniformly bringing the threads to the edge of the impression and on the same section of the drum scale.

4. Physical nature, mechanisms and kinetics of structural transformations in aluminum and alloys based on it

4.1. Mechanical spectroscopy of materials after their mechanical and thermal treatment

A large number of scientific works are devoted to the study of the substructure. In the works [21; 42; 43] the results of studies of substructurally strengthened aluminum and its alloys by the method of mechanical spectroscopy are presented. To obtain the substructure in the materials, according to the polygonization mechanism, the method of mechano-thermal treatment (MTT) was used. The substructure formed in this way is blocked by settling on the dislocation walls of impurity atoms and their clusters. For aluminum and its alloys, appropriate MTT were applied (Table 4.1) [44].

Each of the applied MTT led to a certain polygonal structure, each of which was characterized by the corresponding values of the dislocation parameters and the value of the thermomechanical stability of the strengthening sub-structure.

Table 4.1

MTT of aluminum alloys [44]

Metal or alloy	Deformation temperature, K	Degree of deformation, %	Temperature of polygonization annealing, K	Duration of annealing, min
Al (A999)	293	10	723	30
	423	10	723	30
	523	10	723	30
	923	10-20	903	30
Al-0,01 % Cu	523	10	723	240
Al-0,1 % Cu	523	10	723	840
Al-0,01 % Zn	523	10	723	30
Al-0,1 % Zn	523	10	723	30
Al-0,5 % Zn	523	10	723	480
Al-1,0 % Zn	523	10	723	960
Al (A7)	293	20	903	480
	523	20	903	30
	903	20	903	30

It was found that the redistribution of dislocations as a result of their interaction with each other and with point defects during the transition

of aluminum and its alloys from a highly defective to a thermally more balanced structurally strengthened state causes the appearance of three new inelastic effects in the temperature dependence of IF in the temperature range $473-603\,K$ [42–44]. According to these works, these effects are due to the following processes:

effect $A(493\,K)$ – the interaction of dislocations in the walls with point defects that diffuse along the subboundaries;

effect $B(538\,K)$ – non-conservative movement of dislocations in the walls;

C effect (563 *K*) – the interaction of individual dislocations and their clusters inside polygons with dislocations that form small-angle boundaries.

It is shown that the basis of the processes responsible for effects *A* and *B* is the movement of steps on dislocations, which create subboundaries due to the near-boundary diffusion of point defects and the volume diffusion of vacancies, respectively. The proposed model, allows to explain the mechanism of the *C* effect. It is based on the processes of formation under the action of sign-changing voltage of steps on dislocations located inside subgrains, and the creeping of dislocations from one sub-boundary to another by absorbing or releasing vacancies.

The revealed effects have a relaxation nature (Figure 4.1, a). A change in the frequency of oscillations leads to a clear shift in the temperature of all three peaks *A*, *B*, *C*. The activation energy of the processes that determine their manifestation is determined by the mode of mechanical and thermal processing and is equal to $125\,kJ/mol(1{,}30\,eV)$, $133\,kJ/mol(1{,}38\,eV)$ and $141\,kJ/mol(1{,}46\,eV)$, respectively. With an increase in the deformation temperature at MTT, the peak *A* decreases, and the peak *C* increases and shifts toward high temperatures. Only the magnitude of the peak *B* practically does not depend on the type of MTT. The regularities of the behavior of inelastic effects are revealed depending on the degree of disequilibrium of the initial state, which is determined by the difference in free energies in the given and equilibrium states, on the temperature of deformation during MTT, as well as on the temperature and time of polygonization annealing. The time dependence of these effects during structure stabilization has been established. Metallographic and X-ray analyzes proved that a polygonal substructure with open dislocation walls is responsible for the manifestation of all three peaks in aluminum [44].

At the same time, a certain number of individual dislocations and their clusters are stored inside the polygons. An increase in the temperature of deformation at MTT from 293 to 523 *K* activates the processes of polygonization, as a result of which the detected inelastic effects begin to manifest immediately after deformation. The application of MTT at 903 *K* leads to the complete formation of a more perfect substructure with closed polygonal walls already in the process of deformation, which is characterized by the clearest manifestation of the *C* peak.

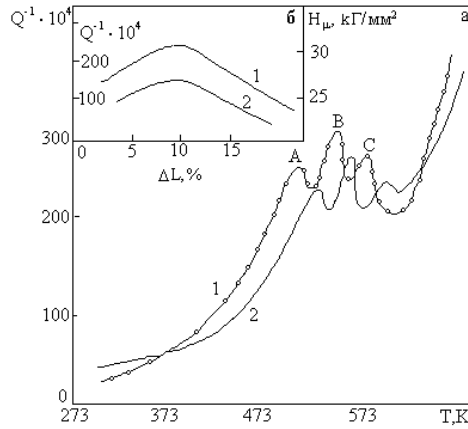

Figure 4.1. Temperature dependence of the internal friction of substructurally strengthened aluminum (a) [43; 44]: 1 – frequency 0,5 *Hz*; 2 – the frequency of 1,4 *Hz* and the dependence of the value of microhardness (1) and the value of the peak *B* (2) on the degree of deformation (b)

The stability of the detected effects is different and is determined by the nature of the substructure, which is obtained by the determined MTT. High-temperature annealing of samples with a formed substructure by MTT methods at 298 *K*, 423 *K*, 523 *K* is accompanied primarily by the removal of individual dislocations and their clusters from the internal volumes into polygonal walls. At the same time, there is a gradual decrease in the *C* effect. The most stable peak after such MTT is the peak *B*. Calculations based on the theory of high-temperature relaxation in subboundaries [42] and experimental data [43] gave the temperature position of the relaxation effect, which is associated with creep of dislocations and coincides with the temperature of manifestation of the effect *B*. High-temperature MTT of the polygonized state, which is characterized by the appearance of the peak B, which is caused by the introduction of fresh dislocations into the internal volumes of polygons, causes the appearance of the effect *C* and its growth with an increase in the

density of dislocations inside polygons. In the initial stages of annealing at the temperature of 573 *K*, this effect decreases according to the dependence:

$$Q^{-1} = f(t^{2/3}) \tag{4.1}$$

where t – is the annealing time.

The determination of the activation energy $E = 12,3\,kJ / mol\,(0,128\,eV)$ and the nature of the time dependence made it possible to associate such a change in the *C* effect with the annihilation of steps on dislocations that arose as a result of high-temperature deformation.

The degree of manifestation of the detected effects, and therefore the perfection of the forming substructure, also depend significantly on the density of dislocations, which is determined by the degree of deformation. The optimal rein-forcing substructure is obtained at a deformation of 8-10%.

A good correlation was established between changes in microhardness and the intensity of manifestation of the *B* effect (Figure 4.1, b) [43]. This gives reason to think that the identification and change of peak *B* in the substructurally strengthened state can serve as an additional method of non-destructive control of its strength properties.

With the help of X-ray structural and metallographic analyses, the average distance between polygonal walls $l = 10^{-3}$ *cm* and between dislocations $h = 10^{-6}$ *cm* was determined. Depending on the type of MTT, the product varies within $10^{-9} – 10^{-11}$ cm^2.

The presence of impurities in the material significantly changes the conditions for the formation of the reinforcing substructure. A decisive role is played by the influence of impurities on the movement of dislocations during sliding and creep. Due to the elastic interaction between dislocations and impurities, the latter block dislocations and, thus, are effective barriers to their movement. Thus, the influence of the copper atoms on the nature of the manifestation of inelastic effects *A, B, C* in the process of formation and stabilization of the substructure was studied in the works [45; 46]. The application of MTT with deformation at 523 *K* showed that the presence of 0,01% *Cu* in-creases the time of polygonization annealing at 723 *K* to 4 hours, and 0,1% *Cu* to 14 hours. The presence of small concentrations of zinc in aluminum causes an intensive growth of the high-temperature background of IF [47; 48]. The content of zinc impurities up to 0,1% does not affect the amount

of polygonization annealing, which is necessary for the formation of the substructure. Larger concentrations of zinc impurities caused an increase in the duration of annealing up to 16 hours.

4.2. Strengthening of metals and alloys by means of the thermocyclic treatments

The methods of forming the strengthening substructure in aluminum and its alloys are different. In pure aluminum, it is possible to form a substructure by the mechanical and thermal treatment. For example, with the help of deformation by 10% at room temperature followed by long-term annealing at 450°C (Figure 4.2, curve 1). However, the application of this treatment to technical aluminum does not lead to the formation of a substructure (Figure 4.2, curve 2). Copper and zinc atoms, as well as impurity complexes contained in technical aluminum, complicate the formation and evolution of the substructure. The substructure can be formed by raising the temperature to 630°C and increasing the duration of polygonization annealing by 16-32 times.

Therefore, dislocations are blocked by impurity atoms and only prolonged annealing at elevated temperatures leads to their redistribution in the subboundary. Using the MTT method, it is impossible to form a

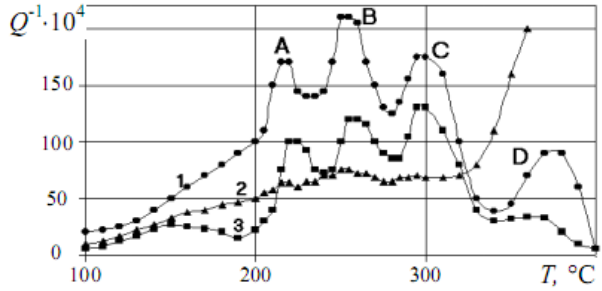

Figure 4.2. Temperature dependence of the internal friction of aluminum. Heating curves after background subtraction after tensile deformation by 10% at 20°C and 32 hours of annealing at 450°C (1), technical aluminum AD1 after stretching by 10% at 20°C and 32 hours of annealing at 450°C (2), technical aluminum AD1 after 36 thermal cycles in the temperature range of 500–20°C [44; 49]

substructure in dispersion-hardening alloys, where dislocations are blocked by impurity atoms, Guinier-Preston zones, and dispersed phases.

Formation of the substructure in such materials can be carried out by repeated thermal cycling (Figure 4.2, curve 3), and especially by thermal cycling in the fields of external stresses (FES).

The TCT method as a method of heat treatment (HT) is based on the continuous accumulation from cycle to cycle of changes in the structure of metals. The change in the structural state and properties of materials during TCT depends on many factors, which can be divided into external and internal [50].

In contrast to standard methods of maintenance, additional sources of action on the structure appear during TCT, which are characteristic only of the process of continuous temperature change, the main of which are phase transformations, temperature gradients, thermal (bulk) and interphase stresses (they are caused by the difference in thermophysical characteristics elements that make up the phase structure). In some cases, all these processes may occur simultaneously, but some of them may be minimized or absent. It depends on the physical nature of the material, mode and purpose of processing. The following TCT methods are possible: thermocycling with full or partial phase recrystallization; thermocycling in the area of variable solubility of elements in each other, as well as processing in the temperature range of dispersion hardening.

All of the above methods are associated with phase transitions of the 1st kind, in which enthalpy, entropy, and microvolume change in leaps and bounds. Depending on the type of movement of atoms across the interphase boundary and the degree of the development of the diffusion processes, the transformations are massive, martensitic, coherent, and normal. All phase transitions are connected with the aspiration of the system to an energetically more favorable state. At the same time, the process of the diffusion of atoms, depending on the nature of the material and its physical and chemical properties, can follow one of the mechanisms mentioned above.

During TCT, not all processes that are characteristic of the heating of the weakly deformed metals occur at the same time. That is, due to the continuity of the temperature changes, some may progress, others may slow down, and others may develop. If the structural components of the

material are not severely deformed, as is the case with TCT, then primary recrystallization may occur in the heating half-cycle, and polygonization may occur at lower temperatures. This leads to the formation of a fine-grained structure.

The authors of a number of works [51–53] studied the nature of changes in the structure and properties, shape and size of samples made of aluminum-based material. It is shown that this is a consequence of the occurrence of internal tensions. Along with the external manifestation of the cycles, there are also internal ones, such as the grinding of grains and their mobility, the formation of a blocky substructure, etc. Grain grinding occurs more than 10 times during thermal cycling of the *Al* – 40% *Zn* alloy at 200 ÷ 357°C [52]. At the same time, the density of dislocations in the aluminum matrix also increases. Grinding of grains in silumin ~12% *Si* is accompanied by the formation of a substructure and disorientation of subgrains during processing at 8 ÷ 340°C. The grains of the silicon phase remain unchanged, and only their mutual arrangement changes due to the deformation of the aluminum matrix [53].

Thermal cycling of cold-rolled aluminum 99,999% *Al* [54] in the regimes of 20 ÷ 400°C and 200 ÷ 600°C leads to recrystallization, which stops as the cycles increase and the process of polygonization develops. It is noted that the cause of stress in pure aluminum is the temperature gradients that are formed during TCT of massive blanks. It was found that in the absence of gradients, the structure of aluminum single crystals practically does not change.

The authors [55] studied the formation of the structure and properties of aluminum alloys (D16, AK6, AK4-1) during high-temperature TCT (HTTT) using the methods of X-ray structural analysis and electron microscopy. It is shown that after HTTT, a developed polygonal intragranular structure with an azimuth-al misorientation angle of several degrees is observed, which is preserved after stamping with subsequent maintenance (tempering and aging).

HTTT of blanks leads to a decrease in the anisotropy of the plastic properties of stamping. At the same time, the warping of parts is reduced by 2-3 times.

The effect of HTTT on powder silumin SAS1-50 [56] showed that the change in the dimensions of parts takes place as a result of the action of

oriented stresses caused as a result of microplastic deformations, which turn into macroplastic ones. The main causes of microplastic deformation are the presence of an oriented strengthening phase and the development of healing processes and the formation of microcracks under the action of interphase stresses. At the same time, HTTT allows to increase the relaxation stability of the alloy by 20-40% The strengthening of the alloy takes place due to the increase in the density of dislocations and the grinding of the silicon phase. Aging of this alloy does not lead to significant strengthening, but on the contrary, can lead (with prolonged heating) to coagulation of the silicon phase and intermetallics.

Thus, TCT regimes differ both in purpose and in the nature of structural transformations, the temperature range of thermocycling, as well as the presence of additional actions. The main tasks of technological regimes of TCT are grinding of the microstructure and spheroidization of excess phases, increase (decrease) in the density of dislocations, relaxation processes, and improvement of physical and mechanical properties.

It was experimentally established that the change in the dispersion of plastic deformations and the coordinate part of the correlation function is related to the development of phase distortion, and the change in the covariance function at zero shear indicates the development of the diffusion relaxation of stresses.

The coordinate component of the correlation function, if its periodicity is neglected, is well confirmed by the experiment and has the form [38]:

$$f\left(r_0\right) = exp\left(-\left(r_0 / d\right)^{0,5n}\right) \tag{4.2}$$

where d – is the average grain size, n – is a coefficient that characterizes the efficiency of TCT.

The average stress $\sigma(n)$, which leads to plastic deformation, will characterize the positive effect of TCT, if the yield strength $\sigma_i = \sigma_{11}$ in the direction of the tensile axis of the sample will increase. The critical stress σ_{11}, which determines the start stress of dislocations, when $n > 1$ is determined by the expression [57]:

$$\sigma_{11} = \sigma_0 + kd^{-0,5n} \tag{4.3}$$

where σ_0 – is the initial value of the yield strength, k – is the coefficient.

Strengthening during TCT is determined by the type of the coordinate part of the correlation function and at a certain stage of TCT can be subject to

Petch's law ($n = 1$). When $n \geq 1$, the process is damped, which is associated with the diffusional relaxation of the concentration stresses.

Thus, by changing the function $f(r_0)$ and the value of σ_{11}, it is possible to find the optimal number of cycles for the strengthening TCT, when the increase in n does not make a significant contribution to the growth of σ_{11} or leads to a decrease in strength. According to the numerical value of n, it is possible to estimate the contribution of plastic deformation of grains during TCT to the overall strengthening effect.

Conducted studies [36] on the experimental determination of structural stresses in *Al – Si* alloys showed that in the half-cycle of heating, the compressive stress on silicon particles (at 20°C) decreases as a result of the anticipatory expansion of the aluminum matrix. Upon reaching a temperature of about 300°C, the voltage in silicon approaches 0, and upon further heating to 530°C, it almost does not change. This type of stress change indicates their constant relaxation when the temperature rises above 300°C due to the deformation of the aluminum matrix.

With the help of X-ray structural analysis, the authors [44] studied the effect of TCT 300 – 400 ÷ 780°C on the structural strengthening of 20XM and 20XZM steels. It is shown that preliminary TCT improves the mechanical properties of steels. Substructural strengthening after TCT allows to increase the strength and impact toughness by about 10%. In order to preserve the positive effect of TCT, it is necessary to limit the exposure time at the austenization temperature and the number of cycles.

The authors of a number of works [50–55] investigated the effect of TCT with other types of physical actions on the formation of the structure and improvement of the properties of metallic materials.

The processing in which the deformation makes major changes in the structure of subsequent or simultaneously occurring phase or structural transformations is called mechanical-thermocyclic (MTT). It is effective both for non-ferrous alloys and steels [20–44]. Due to the effect of deformation, the kinetics of the decomposition of the α-solid solution changes. At the same time, the deformation does not affect the mechanism of subsequent aging, but only changes the speed of its individual stages. In addition, under the influence of deformation, instead of intermittent decay (segregations are formed mainly at grain boundaries), which occurs during aging of undeformed alloys, it becomes continuous and spreads over

the entire volume of grains. In the work [23], heat treatment of aluminum alloys was carried out according to the scheme: TCT before quenching, quenching and aging by TCT in the area of dispersion hardening. In order to increase fatigue life and hardness while maintaining strength and fluidity, TCT during aging was carried out in the range (–130 ÷ 200°C) with a heating rate of (0,3 – 8,0) Ks^{-1} and cooling – (2,0 – 100) Ks^{-1}. The number of thermocycles did not exceed 3-7, and the heating operation in each cycle was combined with the application of ultrasonic vibrations. In addition, after aging, 4-12 TCT were additionally performed in the temperature range 20 ÷ 170°C. And in the work [50], the increase in the fatigue life of steel products was carried out according to the scheme: quenching, low tempering, surface hardening by plastic deformation and cyclic loading followed by tempering. Moreover, cyclic loading followed by tempering was carried out multiple times, and in each subsequent cycle the load amplitude was increased in proportion to the change in the minimum value of the static distribution of microhardness in the zone of predicted failure, according to the equation:

$$\sigma_{in} = \frac{HV_{0n}}{HV_{0(n-1)}} \cdot \frac{K_{er(n-1)}}{K_{er\,n}} \cdot \sigma_{i(n-1)}, \tag{4.4}$$

where $HV_{0(n-1)}$ and HV_{0n} – are the minimum values of the static microhardness distribution before the $(n-1)$ – *th* and n – *th* load; $K_{er(n-1)}$ and $K_{er\,n}$ – are coefficients of load action efficiency.

A large number of works [20; 23; 38] are devoted to the study of the effect of TCT on the structure and physical and mechanical properties of metallic materials by the method of mechanical spectroscopy (IF). Based on the data on the background of IF Q_b^{-1} and elasticity characteristics, taking into account the structural state of the alloys, the authors [20] claim that the TCT (620 – 650 ÷ 800 – 810°C) of 40XA steel leads to an increase in Q_b^{-1} by almost 30% This behavior of IF indicates an increase in the density of dislocations, the grinding of grains and subgrains, and also increases the dissipation of energy during the propagation of ultrasonic vibrations. Grinding of grains and subgrains during TCT leads to the relaxation processes and lowers residual internal stresses of the second kind. For U10A steel, the background IF increases by ~5%. That is, it can be assumed that there are other reasons for the transformations in TCT. A significant

change in Q_b^{-1} as a result of TCT of high-strength cast irons is associated with grinding of grains, spheroidization of cementite, graphitization and redistribution of the main alloying elements.

The authors [23] gave an estimate of the structure of the state of the welds based on the change in the value of Q_b^{-1}. It is shown that the shock viscosity is inversely proportional to the IF background. In addition, the change in the Q_b^{-1} value makes it possible to estimate the duration of welding technological processes and subsequent maintenance. It was established that after TCT the value of Q_b^{-1} does not differ much for different areas of the weld and base metal. This indicates a uniform distribution of mechanical properties and structural stability of the thermally affected zones.

In $Al - Zn$ alloys, already at the beginning of TCT (380 – 390 ÷ 560°C), a significant dissolution of excess phases takes place, and structural changes in stress, which continuously decrease, weaken their effect [44].

The analysis of the structural state after low-temperature thermocycling treatment (LTTT) for *Al – Si – Mg* and *Al – Mg – Zn* alloys is presented in works [36]. A comparison of the amplitude dependences of the IF shows that after the LTTT, the curves are shifted towards larger amplitudes of deformation in comparison with the samples processed by standard technology. The hysteresis after LTTT is also greater, and the value of the critical deformation amplitude ε_1 [36] is 1,75 times greater in the *Al – Si – Mg* alloy and 1,60 times in the *Al – Mg – Zn* alloy in samples after LTTT than after traditional maintenance.

The revealed regularities prove that TCTs significantly improve the structure of metals and alloys; grind and spheroidize phases; contribute to a more complete and uniform dissolution of the chemical elements in a solid solution, increase the density of dislocations; leads to grinding of grains and subgrains [20].

The authors [4; 46] studied the effect of TCT on structural changes in the composite materials with an aluminum matrix reinforced with steel and boron fibers using the method of mechanical spectroscopy. The research results showed additional strengthening of the composite material due to the formation of a dislocation substructure in the aluminum matrix. At the same time, fragile transition zones are formed at the interphase boundary during such treatments.

As can be seen from the considered works, the following are not fully clarified: the formation, behavior and degree of stabilization of the substructure in industrial materials depending on the amount of concentration and nature of impurities and the influence of various physical fields; the sequence and kinetics of the separation of the dispersed phase, and there is no information about the volumetric fate of the separation and the size of the phase particles (except for an attempt to answer this question in papers [4; 23; 46]).

4.3. Temperature dependence of substructurally strengthened aluminum and its alloys

The main factors affecting the kinetics of the process of transition of a material with a high density of dislocations into a metastable state and the character of the obtained substructure are the temperature and the degree of deformation, the temperature and duration of the polygonization annealing, and the TCT parameters. The use of combined processing of materials makes it possible to rearrange the dislocation structure in a configuration such as the boundaries of polygons and cell walls, which will ensure the necessary thermomechanical stability of the strengthened state.

4.3.1. Creating a substructure in pure aluminum

Measurements of TDIF in aluminum were carried out after TCT in FES. The formation of a substructure in pure aluminum was judged by the manifestation of effects *A, B, C* [43–44; 50]. Follows that a large-grained sample was used, and there are no effects in the region of the sublimit peaks (473 – 603 *K*). Just one thermocycle in the FES determines the manifestation of the *A* effect at 503 *K*, an inflection at (553 – 583 *K*), and a clearly expressed *C* effect at 603 *K*. In addition, a small effect is manifested at 453 *K*. Such a manifestation of sublimit effects shows that already at 1 TCT a significant number of free dislocations and their clusters are created in the sample, which cause the appearance of the peak at 603 *K*. Diffusion of the point defects, in the majority of vacancies, along the dislocations causes the appearance of the peak at 503 *K*. Only a bend is observed, then the dislocation walls have not yet formed. But already 5 TCT in FES create a sufficiently developed polygonal structure. This is evidenced by the clear manifestation of all three sublimit effects. The peak *A* practically does not

change at the same time. This indicates that the density of the point defects in the sample changes little. The peak *B* was clearly formed and increased in absolute value by two times. At the same time, the *C* peak increased significantly. The effect at 453 *K* also increased a little. It may be related to partial recrystallization of the sample during heating. The peak *A* at 703 *K* (430°C)was also found on the temperature dependences of IF. Its physical nature is unclear and requires additional research.

The correlation between the change in microhardness and the value of the peak *B* allows us to hope that the identification and change of the peak *B* in the substructurally strengthened material can be an additional method of non-destructive control of the strength properties of the material.

4.3.2. The influence of grain size on the evolution of the substructure in aluminum-based structural materials

According to the theory of dislocations, significant results have been achieved in strengthening materials by redistributing the dislocations themselves into a metastable polygonal structure. The physical nature and kinetics of these processes are successfully studied using the IF method. The difficulties lie in the fact that the substructural effects, with the help of which we judge the nature and state of the substructure, are manifested in the temperature interval (473 – 573 *K*) of a large grain boundary effect. Therefore, in the presence of the grain boundary effect, substructural peaks appear weakly on the very turns of this effect. Thus, all previous studies of substructure formation in pure aluminum were conducted on pseudo-single crystals, which are characterized by the absence of a grain boundary effect. Significant successes have been achieved in this direction, but they do not have direct application, since fine-grained metals and alloys are used in the technology.

The lack of methods for the formation of the dislocation structure in industrial fine-grained aluminum alloys makes it difficult to apply the developed theory to the designs of machine-building equipment. Therefore, in order to prepare for the possibility of practical application of the obtained results, it is necessary to conduct a study of the processes of the formation and stabilization of the substructure in alloys with different grain sizes. And thereby develop the technology of obtaining substructure in fine-grained materials used in technology. The size of the grain was judged by the intensity of the manifestation of the grain boundary peak of IF.

The results of studies of the low-frequency spectrum of elastic energy absorption in dispersion-hardening *Al* – 3% *Zn* and *Al* – 3% *Cu* alloys during their thermocycling in the equilibrium and stressed states are shown. Sample processing was carried out according to the methodology given in the work.

The first feature of the obtained results is that the grain-boundary peak of IF appears at a temperature of 633 – 653 *K*. This circumstance determined favorable conditions for further studies of substructure formation in polycrystalline samples. Such a shift of the grain boundary peak from 553 *K* led to its manifestation outside the temperature range of the detected substructural effects of 493 – 603 *K*.

The initial state of the studied *Al* – *Zn* alloys was characterized by the appearance of a large grain boundary peak at 633 *K* and an impurity grain boundary peak at 693 *K*. The grain size of this sample was about 0,3 *mm*. Thermal cycling was carried out in the temperature range of 273 – 793 *K* under a load of $0,2_{\sigma_{0,2}}$. Such processing of the alloy determined the formation of a polygonal structure. At the same time, it is characteristic that at the beginning of TCT among the substructural effects, the peak *B* and especially the peak *C* were better manifested. The peak *A* was not manifested at all. The absence of this peak is probably due to the fact that point defects (impurities and vacancies) are concentrated mainly on grain boundaries. It is energetically more beneficial for them to be there. The peak *B* is poorly manifested, since the substructure has not yet formed.

At the same time, the appearance of the *C* peak, which is connected with the interaction of individual dislocations and their clusters located inside the polygons, with the polygonal walls, becomes completely incomprehensible. It can be assumed that not only the interaction of individual dislocations and their clusters with the dislocation clusters, but also with large-angle grain boundaries is responsible for the appearance of the peak *C*. Therefore, in this case, the *C* peak is caused by the interaction of individual dislocations and their clusters with large-angle grain boundaries. The subsequent increase in the number of thermocycles leads to a gradual improvement of the dislocation structure.

At the same time, all three effects are manifested on the curve of temperature dependence of IF. The peak *A* is very well formed. It indicates a developed substructure. At this time, the peak *C* continues to manifest

itself well. It has become somewhat wider, which also speaks in favor of the physical nature of this effect. At the same time, the effect on the temperature dependence of IF in the region of low temperatures is manifested at 333 *K*, 393 *K*, and 433 – 453 *K*. The first two are due to the dissolution of GP zones, and the third is due to Zener relaxation. We can see that the formation of the substructure by the TCT method under load was successfully carried out in both cases, but the nature of the manifestation of the sublimit peaks is significantly different.

Thus, effect *B*, which is associated with the non-conservative motion of dislocations, depends little on the grain size. At the same time, with an increase in grain size, the *C* peak increases significantly. This confirms the assumption about its physical nature, but taking into account the fact that the contribution to energy dissipation, in the case of its manifestation in a polycrystal, is due to the interaction of individual dislocations and their clusters with subgrain boundaries, and not grain boundaries. This is supported by a significant broadening of the *C* peak in the case of a polycrystal, which indicates the occurrence of processes with different relaxation times. It is also interesting that the effect *A* increases with increasing grain size. This may be due to the fact that in the case of a polycrystal, the main part of impurities is located along the grain boundaries and there are no conditions for the manifestation of the peak *A*. As the grain size increases, the length of the grain boundaries decreases and part of the impurities goes into the internal volumes of the grain, where it settles on the subboundary and, diffusing in them, causes the manifestation of effect *A*.

Sublimit effects behave somewhat differently during thermal cycling of polycrystalline *Al* – 3% *Cu* samples. As can be seen from Figure 4.3, b, the sublimit effects manifest themselves rather poorly on polycrystalline samples. Moreover, with an increase in the number of thermocycles, all three effects generally decrease. At the same time, the *C* effect also expands and shifts towards high temperatures. As for *Al – Zn* alloys, in polycrystalline *Al – Cu* alloys, when the substructure is formed, the *C* peak manifests itself better.

For a polycrystal, substructural effects are manifested better than in a large-grained sample. This is due to the fact that in polycrystals with long grain boundaries, impurities of the copper atoms settle on the grain boundaries and release internal dislocations that take part in the formation

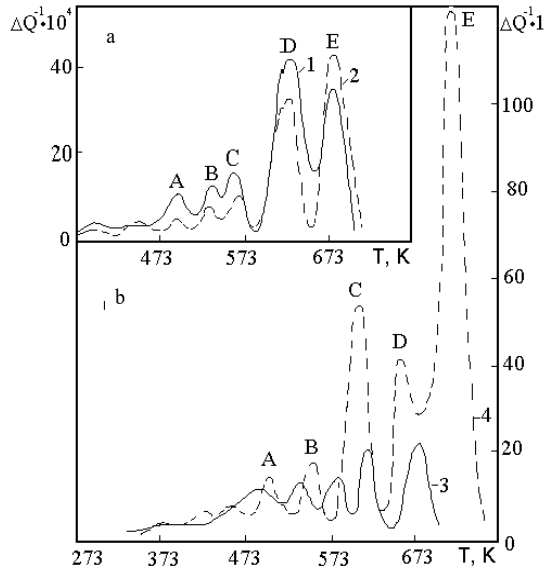

Figure 4.3. TDIF of the polycrystalline *Al* – 3% *Cu* after 9 TCT in FES; 2 – after 24 TCT in FES; (b): 3 – large-grained sample after 9 TCT in FES; 4 – polycrystal after 39 TCT in FES [50; 51]

of the strengthening substructure. As the grain size increases, part of the copper atoms moves inside the grain and effectively blocks dislocations. This limits their mobility and prevents the formation of the substructure.

Thus, the results of studies of the temperature dependence of IF of substructurally strengthened *Al – Zn* and *Al – Cu* fine-grained alloys showed that the grain boundary and impurity grain boundary effects are shifted to the region of high temperatures and are manifested in the range of 633 *K* and 693 *K*. This makes it possible to thoroughly study the substructural effects, which appear in the temperature range of 473 – 603 *K*. In addition, this method of forming and stabilizing the substructure in aluminum-based industrial alloys also affects the grain size. In most cases, an increase in the amount of TCT leads to the grain refinement, but this dependence is not proportional.

4.3.3. Substructural strengthening of dispersion-hardening *Al* – 4% *Cu*, *Al* – 4% *Zn*, *Al* – 4% *Cu* – 6% *Zn* alloys

The influence of impurities on the processes of formation and stabilization of the structure is reflected in the behavior of inelastic effects *A*, *B*, *C*, which have a relaxation nature and are connected with the interaction and redistribution of dislocations and point defects in the process of formation and stabilization in the material of a polygonal structure.

The activation energy of the processes causing their manifestation is 1,30, 1,38 and 1,45 *eV*, respectively. The degree of their manifestation is determined by the heat treatment regime. The choice of copper and zinc impurities is caused by the fact that the *Al* – 4% *Cu* and *Al* – 4% *Zn* systems belong to the dispersion-hardening alloys. Therefore, prerequisites are created for further studies of the possibilities of fixing the dislocation structure not only by individual impurities or atoms, their clusters, but also by dispersed allocations. The possibilities of combining two different directions of achieving a strengthened state by means of the creation of a substructure and allocation of a dispersed phase should serve as a new promising stage of obtaining a high-strength state of materials.

The influence of copper atoms on the nature of the manifestation of inelastic effects *A*, *B*, *C* [44; 50] in the process of formation and stabilization of the substructure is shown in Figure 4.6 for *Al* – 4% *Cu* alloy. Before thermal cycling, the $Q^{-1} = f(T)$ curve shows a small grain boundary effect at 623 – 693 *K* and an impurity grain boundary peak around 673 – 693 *K* (Figure 4.4. a, curve 1). Already one thermal cycle (Figure 4.4. a; curve 2) creates an increased concentration of defects in the crystal structure, and heating this sample under load causes their redistribution and manifestation of substructural effects: *A* at 493 *K*, *B* at 553 *K* and *C* at 598 *K*. In addition moreover, a peak appears at 453 *K*, which is associated with the recrystallization of the sample. The manifestation of the substructural effects *A* and *B* indicates an intensive process of polygonization in the loaded state due to the redistribution of dislocations in the walls and the diffusion of distant point defects in the walls. At the same time, the grain-boundary effect increases and shifts toward low temperatures, which indicates grain crushing during TCT in FES. It follows from the analysis of $Q^{-1} = f(T)$ that the dependence of substructural effects on the amount of HTTT is oscillatory (Figure 4.6, b).

The period of these processes after TCT without load is 30 cycles; and after TCT in FES, the process of changing effects is reduced by 2 times. As can be seen from Figure 4.4, b values of sublimit effects with an increase in the number of thermocycles oscillate with a decaying amplitude. Stabilization of sublimit effects takes place after 60 TCT.

The results of the effect of zinc atoms (*Al* – 4% *Zn* alloy) on the dependence of $Q^{-1} = f(T)$ after HTTT in FES are shown in Figure 4.5. In addition to substructural effects *A*(513 *K*), *B*(553 *K*) and *C*(603 *K*), peaks at 353 *K*, 393 *K*, 453 *K*, 633 *K*, 693 – 703 *K* are observed (Figure 4.5, a). Their comprehensive study and comparison with literature data give reason to assume that they are related to such processes, the effects of which at 353 *K* and 393 *K* are associated with the dissolution of Guinier-Preston (GP) zones; effect at 453 *K* due to recrystallization of the sample; effects at 633 *K* and 693 – 703 *K* are grain boundary and impurity grain boundary, respectively.

Studies have shown that during the formation of the substructure and the settling of individual atoms of impurities of their clusters or phase separations on the dislocation walls, the substructure is effectively blocked, becomes weaker, and the relaxation effects are weaker (Figure 4.5. a, curve 2). An increase in the number of thermocycles to 5 (Figure 4.5. and curve 3) causes, in addition to a sharp increase in peak *C*, the formation of peak *B* at the place of the previous inflection.

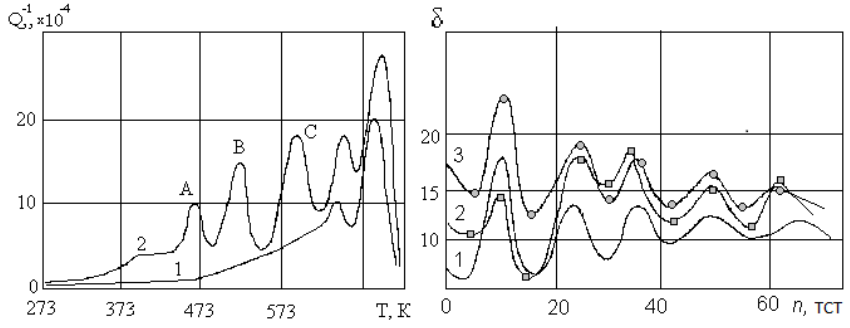

a *b*

Figure 4.4. The nature of the change in substructural effects for alloy 1 at HTTT in FES:
a) 1 – 0 TCT; 2 – 15 TCT; b) 1 – effect *A*; 2 – effect *B*; 3 – effect *C*

Analysis of the temperature dependence of IF of *Al – Zn* alloys shows that, as in *Al – Cu* alloys, the dependence of substructural effects has an oscillatory character (Figure 4.5, b). The oscillation period is 15 TCT. The behavior of the effects *A* (curve 1) and *B* (curve 2) practically repeat each other. It should be noted the anomalous behavior of the effect *C* (curve 3). Thus, the period of its oscillation reflects the periods of changes of the first two effects, but the nature of its behavior is completely opposite. The reduction of *A* and *B* effects is associated with the deposition of impurity atoms on the dislocation walls, which stabilize the substructure.

At the same time, internal dislocations become more mobile and efficiently dissipate elastic energy. This is accompanied by an increase in the *C* peak. An increase in the dislocation density during HTTT contributes to the transformation of low-angle grain boundaries into high-angle grain boundaries. Partial grain crushing occurs, which is indicated by an increase in the peak at 635 *K*.

The subsequent increase in the number of thermocycles causes the accumulation of the defects in new grains and the formation of a new, finer substructure begins. The presence of a well-developed system of subboundaries creates conditions for the separation of some impurities

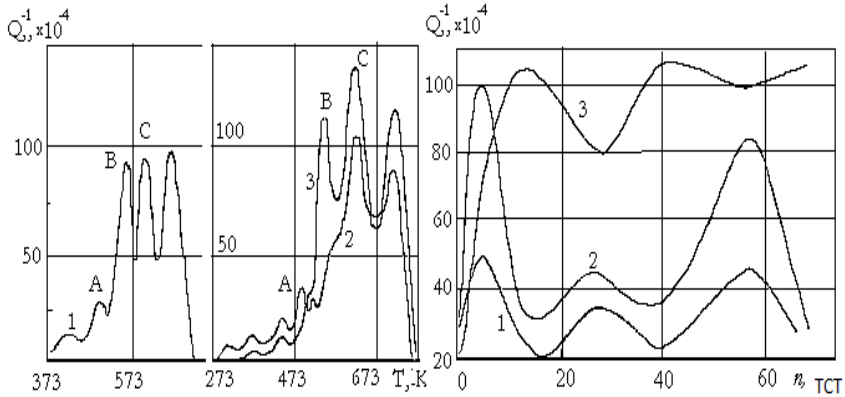

a *b*

Figure 4.5. The nature of the change in substructural effects for alloy 2 with HTTT in FES: a) 1 – 0 TCT, 2 – 5 TCT, 3 – 15 TCT; b) 1 – effect *A*, 2 – effect *B*, 3 – ефект *C*

along the subboundaries. At the same time, the number of impurities at high-angle boundaries decreases, which leads to a decrease in the impurity grain boundary peak at 693 – 703 *K*.

The nature of the structural changes and their evolution during TCT is evidenced by a change in the parameters of the dislocation structure (Table 4.2).

The dislocation density ρ, the length of the L_N dislocation segment was determined from the experimental data of the amplitude dependence of IF and X-ray structural analysis on a computer. Thus, with TCT in FES, the maximum value of the dislocation density ρ and the minimum value of the value of L_N is reached during the first 15-25 TCT, and with HTTT without load – during 35-45 TCT (see Table 4.2). The further increase of thermocycles leads to a decrease in the value of ρ and a slight increase in L_N, at HTTT without load.

Table 4.2

The second critical deformation amplitude, the tangent of the angle of inclination of the background amplitude dependence and microhardness after TCT

Alloy	Heat treatment	Measured value *	Number of cycles					
			0	5	20	25	50	60
Al – 4 % Zn	TCT	2	0,65	0,25	0,46	0,47	0,90	1,0
		3	192,0	260,1	350,3	360,2	230,0	218,4
Al – 4 % Cu	TCT	1	6,0	8,2	9,6	12,0	14,2	14,0
		2	0,7	0,7	0,39	0,23	0,30	0,10
		3	194,0	280,5	382,4	387,2	256,3	203,3
Al – 4 % Cu – 6 % Zn	TCT	1	4,0	6,2	11,5	6,1	8,9	8,7
		2	0,9	1,5	1,33	0,96	0,9	1,9
		4	2,1	10,2	10,2	6,2	9,1	11,1
		5	4,9	2,9	2,9	3,9	2,9	2,9

*** 1 – $\gamma_{cr.2}$,$\times 10^{-5}$; 2 – *tgΘ*; 3 – H_μ, *MPa*; 4 –ρ,$\times 10^{-12} \cdot m^{-2}$; 5 – L_N,$\times 10^{-6}$ m.**

Evidence of strengthening of alloys during TCT is a change in the second critical deformation amplitude $\gamma_{cr.2}$, the tangent of the angle of inclination of the background of the amplitude dependence of IF ***tgΘ*** and microhardness $H_{1/4}$, (see table 4.2).

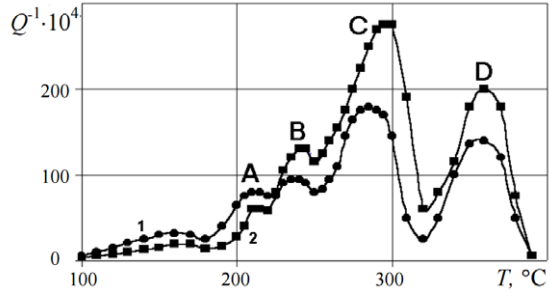

Figure 4.6. Temperature dependence of the internal friction of the *Al* – 4% *Cu* – 6% *Zn* alloy after subtracting the background after 35 thermocycles from 200 to 20°C (1), after 16 thermocycles from 200 to 20°C under a load of $0{,}2_{\sigma 0{,}2}$ (2) [49]

Figure 4.6. shows the influence of thermocycling treatments on the change in the substructural effects of *A, B, C* alloy (*Al* – 4% *Cu* – 6% *Zn*).

In order to confirm the physical nature of the detected effects, the temperature of the manifestation of the effect caused by dislocation creep was calculated based on the theory of high-temperature relaxation of dislocations in subboundaries [44]. The relaxation time of such a process is determined by the ratio:

$$\tau = \eta / \chi, \tag{4.5}$$

where η – is the effective viscosity coefficient, χ – is the quasi-elastic coefficient, which is equal to:

$$\chi = \left(b^2 \mu\right) / (Lh), \tag{4.6}$$

where μ – is the shear modulus, b – is the Burgers vector, L – is the distance between walls, h – is the average distance between dislocations in the walls. On the basis of (4.5-4.6) we get:

$$Lh = \left(b^2 \mu\right) / \left(2\pi\nu\eta\right), \tag{4.7}$$

de ν – is the frequency of oscillations. The calculated value of $Lh = 6 \cdot 10^{-9}\, cm^2$.

This coincides with the values $L = 10^{-3}\, cm$, $h = 10^{-6}\, cm$ obtained on the basis of X-ray and metallographic studies [44].

With known L and h, it is possible to calculate the factor τ_0 [44] at 265°C.

$$\tau_0 = \frac{kT \ln\left(\frac{h}{2\pi r_0}\right)}{5\mu\Omega D_0}. \qquad (4.8)$$

With $D_0 = 1,7\,cm^2/s$, $\Omega = 10^{-23}\,cm^3$ and $\ln\left(\frac{h}{2\pi r_0}\right) = 5$ we get $\tau_0 = 1,4 \cdot 10^{-11}\,s$. Whence, from the condition of obtaining the maximum internal friction $\omega\tau = 1$, where $\tau = \tau_0\, exp\left(U/\left(kT\right)\right)$, we find the expression for determining the temperature of the manifestation of the effect caused by creeping dislocations:

$$T = \frac{U}{k \ln\left(\frac{1}{2\pi\nu\tau_0}\right)} \qquad (4.9)$$

On the basis of this formula, we obtain that the temperature of manifestation of the relaxation effect caused by dislocation creep in the subboundaries is in the region of 260 – 300°C. This coincides well with the temperature at which effect *B* appears, thereby confirming its physical nature.

Therefore, TCT in a stressed state ensures acceleration of the achievement of a more strengthened state and extension of the interval of preservation of increased operational characteristics of the material.

The joint effect of elevated temperature and stress fields contributes to the redistribution of the defects and the formation of a thin, more balanced, and therefore stable substructure. The variation of the parameters of HTTT in FES opens up wide possibilities of purposeful management of the processes of structure formation, which means obtaining the necessary operational characteristics of the material.

4.4. Parameters of ADIF and substructures of aluminum alloys

The strength and plasticity of crystals are largely determined by their dislocation structure. Dislocations in crystals under the influence of external fields (mechanical loads, temperature, irradiation, etc.) interact with each other and form different spatial configurations. The density of dislocations and the nature of their location in the crystal determine its physical and mechanical properties.

In this paper, an assessment of the determination of the parameters of the dislocation structure and characteristics of ADIF is made based on the curves of the amplitude dependence of damping in dispersion-hardening aluminum alloys.

Aluminum alloys *Al* – 1,3,4% *Cu*, *Al* – 1,3,4% *Zn*, *Al* – 4% *Si* – 1% *Zn*, *Al* – 4% *Si* – 6% *Zn* were selected for the study [56; 57; 58]. When choosing materials, it was taken into account that additional strengthening can be achieved in these alloys due to the creation of a substructure and its stabilization by the separation of a dispersed phase.

To create a developed substructure in the studied materials, thermocycling was carried out in the temperature range (783 ÷ 283 *K*) with a heating and cooling rate of 50 $K \cdot s^{-1}$. The field of external tensile stresses (FES) was (0,4 – 0,6) $\sigma_{0,2}$. Internal friction was measured on a low-frequency (~1 s^{-1}) device of the inverted torsional pendulum type [27; 29; 30].

Figures 4.7, 4.8, 4.9 show the results of ADIF after 20 TCT (curve 1) and 20 TCT in FES (curve 2) for *Al* – *Cu*, *Al* – 4% *Cu* – 6% *Zn* alloys (the graphs are similar for *Al* – *Zn* alloys).

The comparison of ADIF shows that after TCT in FES, the curves are shifted towards larger deformation amplitudes compared to samples processed during thermocycling without load. The mismatch of the curves in the "loading – unloading" cycle, that is, the appearance of hysteresis, indicates irreversible changes in the structure of the material that occur in the

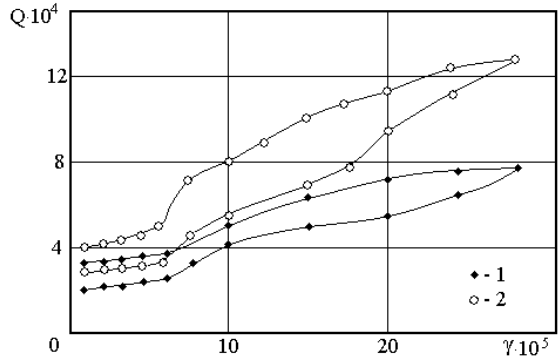

Figure 4.7. ADIF of *Al* – 1% *Cu* alloy after 20 TCT (1) and 20 TCT in FES(2)

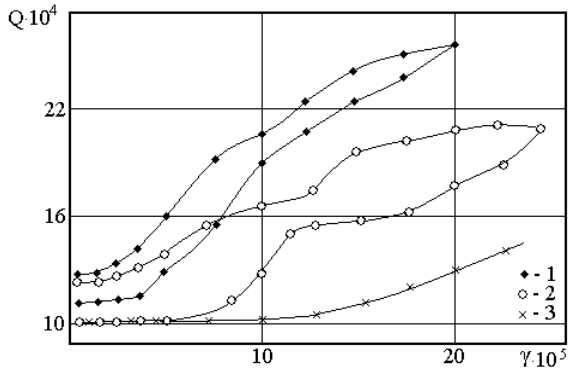

Figure 4.8. ADIF of *Al* – 4% *Cu* alloy after 20 TCT (1), 20 TCT in FES (2) and the background of internal friction (3)

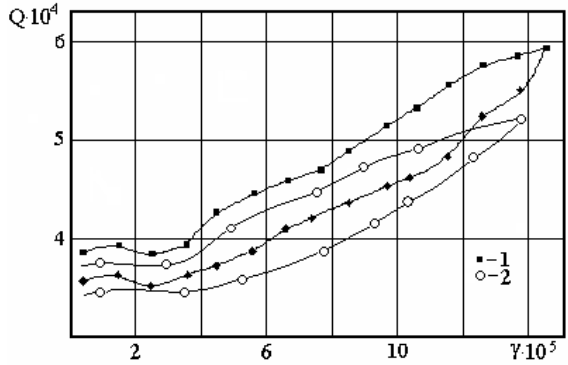

Figure 4.9. ADIF of *Al* – 4% *Cu* – 6% *Zn* alloy after 20 TCT (1) and 20 TCT in FES (2)

process of measuring IF. IF hysteresis after TCT in FES is greater than after thermocycling without load. A large hysteresis after TCT in FES indicates a significant anchoring of dislocations atmospheres of impurities [59]. For *Al* – 1% *Cu*, *Al* – 4% *Cu*, *Al* – 1% *Zn* and *Al* – 4% *Zn* alloys after TCT in FES, this value is equal to 0,75, 0,80, 0,70 and 0,76, and after TCT without load – 0,25, 0,40, 0,35 and 0,38, respectively. For alloys *Al* – 4% *Cu* – 6% *Zn*, *Al* – 4% *Cu*, this value is equal to 0,89 and 0,83, respectively.

The value of the second critical amplitude of deformation $\gamma_{cr.2}$ after 20 TCT in FES, which characterizes the process of propagation and movement of dislocations in a solid solution according to the Frank-Reed mechanism [59], is 1,22 – 1,64 times greater than after 20 cycles of conventional TCT (see Tables 4.3, 4.4, Figures 4.7, 4.8, 4.9).

Substructural strengthening is characterized by an intense increase in the density of dislocations Λ, which are blocked by impurities during dispersion hardening. With equivalent amounts of thermocycling, the density of dislocations under TCT conditions in FES grows 1,2 times more intensively than with conventional thermocycling (Tables 4.3, 4.4).

The development of the dislocation structure during thermal cycling is accompanied by a sharp decrease in the length of the dislocation segments between the anchoring points on the dislocation lines (L_n) and between the nodes of the dislocation grid (L_s). Such data were obtained from the results of measuring the amplitude dependence of IF with their subsequent processing according to the Koehler-Granato-Lucke and Swartz-Wirtman models [5; 6] (Figure 4.10, Tables 4.3, 4.4).

The decrease in the L_c and L_n parameters after TCT in the FES indicates a significant grinding of the dislocation network. This structural state of metals is characterized by high energy capacity and their ability to more evenly distribute external stresses throughout the volume of materials or technical structures from them, which, in combination with the increased level of thermal stability of blocked sub-boundaries, leads to a sharp increase in resistance to plastic deformation at room and elevated temperatures.

After obtaining the values for C_1 and C_2 and using them according to the GL theory [6], we have the opportunity to calculate the parameters of the dislocation structure of materials.

An important physical characteristic of the state of the dislocation structure and the solid solution of the studied material is the condensation temperature T_c – saturated dislocation atmospheres, which characterizes the degree of blocking of dislocations.

Experimentally, the condensation temperature was determined by the onset of the temperature dependence of the first critical deformation amplitude $\left(\gamma_{cr.1} = f(t)\right)$.

Research results show that TCT and external load fields significantly influence the kinetics of dislocation substructure development. Thus,

Table 4.3

Parameters of substructure and ADIF from the number of TCT and TCT in FES for *Al – Cu*, *Al – Cu – Zn* alloys

Alloy	Heat treatment	Measured size	0 TCT	5 TCT	10 TCT	20 TCT	40 TCT	60 TCT
Al-wt. 1 % Cu	TCT in FES	$\Lambda \cdot 10^{-12}$, m^{-2} $L_n \cdot 10^6$, m	1,30 2,90	7,9 2,35	10,1 2,10	26,06 2,04	31,0 1,70	22,1 1,50
	TCT	$\Lambda \cdot 10^{-12}$, m^{-2} $L_n \cdot 10^6$, m	1,10 2,91	5,1 1,75	5,6 1,81	7,20 1,80	17,7 1,33	16,7 1,35
Al-wt. 3 % Cu	TCT in FES	$tg\Theta$	0,70	0,25	0,23	0,23	0,35	0,51
	TCT	$tg\Theta$	0,65	0,35	0,25	0,25	0,45	0,57
Al-wt. 4 % Cu	TCT in FES	$\gamma_{cr.2} \cdot 10^5$ $tg\Theta$ $\Lambda \cdot 10^{-12}$, m^{-2} $L_n \cdot 10^6$, m	6,8 0,71 5,20 5,50	7,1 0,32 8,58 2,46	10,3 0,28 15,6 1,45	13,5 0,25 18,5 2,03	14,0 0,22 28,05 2,46	13,3 0,31 23,5 2,40
	TCT	$\gamma_{cr.2} \cdot 10^5$ $tg\Theta$ $\Lambda \cdot 10^{-12}$, m^{-2} $L_n \cdot 10^6$, m	6,8 0,70 5,02 5,04	7,0 0,39 7,80 3,65	10,0 0,38 8,55 3,50	12,3 0,37 13,50 2,65	14,0 0,39 17,50 2,20	13,6 0,40 16,0 3,10
Al-wt. 4 % Cu-wt. 6 % Zn	TCT in FES	$\gamma_{cr.2} \cdot 10^5$ $tg\Theta$ $\Lambda \cdot 10^{-12}$, m^{-2}	6,2 1,10 4,08	7,5 0,92 5,71	11,2 0,63 8,95	12,8 0,28 13,6	13,3 0,23 18,2	13,0 0,25 17,8
	TCT	$\gamma_{cr.2} \cdot 10^5$ $tg\Theta$ $\Lambda \cdot 10^{-12}$, m^{-2}	6,0 1,09 4,08	7,4 0,95 5,60	8,8 0,73 9,05	9,3 0,41 12,3	10,1 0,33 16,1	10,0 0,30 15,8

Table 4.4

Parameters of substructure and ADIF from the number of TCT and TCT in FES for *Al – Zn* alloys

Alloy	Heat treatment	Measured size	0 TCT	5 TCT	10 TCT	20 TCT	40 TCT	60 TCT
Al-wt. 1 %Zn	TCT in FES	$\gamma_{cr.2} \cdot 10^5$ $tg\Theta$ $\Lambda \cdot 10^{-12}$, m^{-2} $L_n \cdot 10^6$, m	4,1 0,93 2,10 6,21	6,3 0,90 5,1 4,0	8,1 0,83 5,5 4,0	9,2 0,72 7,80 3,65	9,3 0,75 10,3 4,2	10,0 0,86 10,3 3,1
	TCT	$\gamma_{cr.2} \cdot 10^5$ $tg\Theta$ $\Lambda \cdot 10^{-12}$, m^{-2} $L_n \cdot 10^6$, m	4,0 0,90 2,11 4,90	5,8 0,87 3,6 3,1	6,9 0,87 9,1 2,50	7,3 0,85 7,3 2,90	8,0 0,82 10,2 3,23	7,9 0,83 11,1 2,96
Al-wt. 3 % Zn	TCT in FES	$\gamma_{cr.2} \cdot 10^5$ $tg\Theta$	4,3 0,78	7,8 0,45	9,1 0,38	9,0 0,39	8,90 0,39	8,9 0,38
	TCT	$\gamma_{cr.2} \cdot 10^5$ $tg\Theta$	4,4 0,69	5,1 0,60	6,6 0,55	7,9 0,43	8,6 0,40	8,7 0,40
Al-wt. 4 % Zn	TCT in FES	$\Lambda \cdot 10^{-12}$, m^{-2} $L_n \cdot 10^6$, m	3,46 6.50	4,05 5,05	9,90 2,90	12,3 2,83	10,2 3,05	9,36 3,60
	TCT	$\Lambda \cdot 10^{-12}$, m^{-2} $L_n \cdot 10^6$, m	3,50 6,31	3,56 6,0	5,6 3,03	7,95 2,98	10,36 2,96	10,3 3,05

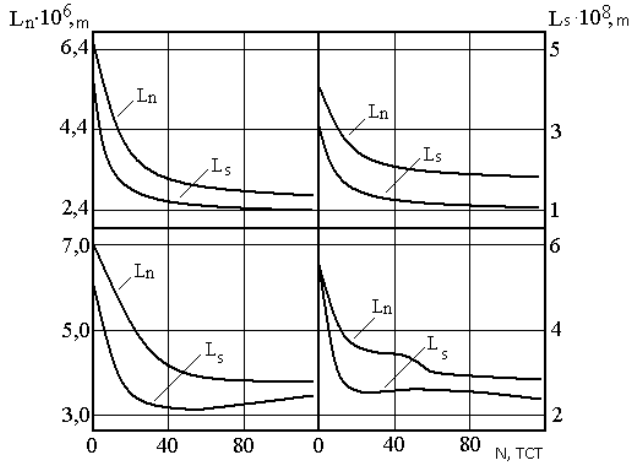

Figure 4.10. The change in the geometric parameters of the dislocation structure of aluminum alloys depending on the amount of TCT in the FES:
a) ***Al – wt.*4%** ***Cu – wt.*6%** ***Zn*****; b)** ***Al – wt.*4%** ***Cu;***
c) ***Al – wt.*4%** ***Cu – wt.*1%** ***Zn*****; d)** ***Al – wt.*4%** ***Zn***

the elimination of the point defects and microplastic deformation, which accompany intense thermal changes, lead to the development of the dislocation structure, and the increased temperature contributes to the rearrangement of dislocations with the formation of polygon boundaries.

The nature of the change in T_c depending on the amount of TCT in the FES correlates with the change in the tangent of the angle of inclination of the ADIF($tg\Theta$) background, which characterizes the intensity of dislocation separation from the anchoring points, as well as the second critical amplitude of ADIF ($\gamma_{cr.2}$) deformation, since an increase in T_c and $\gamma_{cr.2}$ a decrease $tg\Theta$ characterizes an increase in the elastic limit material [57–59].

Thus, measuring the amplitude dependences of IF at various stages of sub-structural strengthening of metals allows us to reveal the general regularities of the formation, stabilization, and decay of networks of polygonal boundaries, the state of which directly determines the level

and stability of high-temperature properties. The data of substructural strengthening of DHA by the TCT method in FES indicate the prospects of thermocyclic substructural strengthening of metals and alloys, which, due to the specific properties of polygonal substructures, not only increases the level of operational properties and resistance to brittle fracture under normal conditions, but also high heat resistance with an increase in the longevity of operation under load conditions at normal and high temperatures.

Such progressive technologies will have a significant advantage as they can be applied not only to materials and alloys as raw materials, but also to ready-made parts or mechanical structures made of them.

4.5. The behavior of mechanical characteristics of structural materials during the development of substructures

The formation and stabilization of the dislocation substructure in aluminum and its alloys primarily pursues the goal of increasing their physical and mechanical properties. The use of these materials in mechanical engineering requires the provision of stable, enhanced properties in a wide temperature range.

The dynamic shear modulus was calculated according to the formula:

$$G = 4\rho l^2 \frac{R(n)}{n^2} K_T f^2, \tag{4.10}$$

where n – is the harmonic number (calculated values of $R(n)$ for samples with a rectangular and round cross-section are well known ($R(n) = l$)); K_T – is a calculated coefficient that takes into account the temperature conditions of research and geometric ratios; ρ – material density; l – sample length.

This work presents the results of studies of the modulus of elasticity and microhardness of dispersion-hardening alloys *Al – Cu – Zn* and *Al – Cu*, *Al – Zn* after thermocycling (TCT). TCT was carried out in the temperature range (520 ÷ 20)°C with a heating and cooling rate of $50\,K{\cdot}s^{-1}$. The external tensile load was $(0{,}2-0{,}65)\sigma_{0,2}$. Creep deformation did not exceed 0,1%.

The value of f^2 of the annealed sample gradually decreases with increasing temperature.

No effects on the dependence $f^2 = f(T)$ are observed. But as the amount of TCT in FES increases, i.e. as the dislocation structure forms in it, the effect on the dependence $f^2 = f(T)$ begins to manifest itself in the temperature range of 220–330°C.

The location of this effect coincides with the temperatures of manifestation of the substructural effects *A*(210 –220°C), *B*(265 – 280°C) and *C*(310 – 330°C) of internal friction (IF). At the beginning, this effect manifests itself in the form of a minimum at temperatures of 260–270°C. With an increase in the number of thermocycles, it shifts to the side of high temperatures. Further, this minimum begins to be preceded by a small maximum, which increases with the growth of the number of thermocycles. Thus, at 10 TCT, it is formed into a well-defined peak at 260–270°C. The next 10 TCT successively strengthen the detected effects. After 19 TCT, they reach maximum values. Given that the decline of the shear modulus with increasing temperature is a normal classical phenomenon, two regions with shear modulus anomalies can be distinguished on this dependence, namely 200–280°C and 320–420°C. In these temperature ranges, the shear modulus increases with increasing temperature. These data indicate the strengthening of the material with increasing temperature [1].

A further increase in the number of thermocycles up to 30 gradually reduces the manifestation of these effects. The next thermocycling up to 50 TCT again activates the manifestation of the studied effects. Then they begin to decrease, and by approximately 60 TCT we again obtain the dependence that characterizes the initial state. Therefore, the regularities of changes in the temperature dependence of the shear modulus of *Al – Cu* alloys, and therefore the regularities of the processes of substructure formation in the TCT process, are periodically repeated with a period of about 15-25 cycles.

The patterns of changes in the temperature dependence of the shear modulus of the *Al – 3% Zn* alloy are approximately similar. They are especially clearly manifested after TCT.

In contrast to *Al – Zn* alloys, in *Al – Cu* alloys there is an additional effect at 433 – 453 *K*, which is associated, apparently, with the previous selection of Guinier-Preston zones.

Studies have shown that the shear modulus undergoes significant changes at the temperatures of formation and stabilization of the changing substructure, the maximum value of the shear modulus is reached after 30-40 TCT. The subsequent increase in the number of thermocycles leads to a decrease in this value. The intensity of the shear modulus change is determined by the degree of disequilibrium in the structure of the materials

under study. In addition, such a change in the value of $G(f^2)$ indicates an increase in the heat resistance of the substructurally strengthened materials.

Therefore, with the help of the obtained results $f^2 = f(T)$ and $f^2 = f(N)$ it is possible to scientifically justify the processing technologies of the studied materials, as well as foresee the dangerous temperature-time conditions of operation of structures made of the substructurally reinforced materials.

Microhardness, which characterizes the energy of the interatomic bond of a crystal, its mechanical strength, or the resistance of the crystal lattice to large plastic deformations and destruction, was chosen as a control characteristic when studying the results of TCT.

Comparing the expressions for describing the dependence of Mayer hardness and lattice energy allows us to conclude that with the same valence and the same lattice current, the hardness is higher, the smaller the distance between the ions. In the case when the interatomic distances are the same, the hardness is higher, the higher the valence.

Therefore, as a direct measure of the hardness of crystals, you can use the ratio of the lattice volume to the molar volume for a given crystal.

Thus, the value of the hardness of different crystals with different crystallographic structures can be quantitatively compared with each other, which results from the atomic properties of the crystals. So, for example, it is known that the transition from less densely packed to more densely packed modifications is accompanied by a change not only in hardness, but also in modulus of elasticity and other characteristics [60].

As experiments have shown, the dependence of the diameter of the impression d on the load P: has a parabolic character: $P = a \cdot d^n$, where *a* and *n* – are constants. In logarithmic coordinates, a linear relationship between *ln P* and *ln d* can be obtained, and the constant *ln a* plays the role of the extrapolated yield strength σ_0, and the constant *n* plays the role of the strengthening coefficient.

The general regularities of the behavior of H_μ and *n* values after TCT for aluminum alloys with different concentrations of copper and zinc were revealed (Tables 4.5, 4.6).

The first 15-40 TCT cause, depending on various heat treatment factors, an increase in microhardness H_μ and a decrease in *n* (see Tables 4.5, 4.6).

It is necessary to note the anomalous nature of microhardness behavior for *Al* – 2% *Cu* alloy. So, for example, the first 7-10 TCT decrease the

Table 4.5

Dependence of microhardness, increase in microhardness H_μ and Mayer index of *Al – Cu* alloys from the number of thermocycles

Alloy	Heat treatment	Measured size	0 TCT	5 TCT	10 TCT	20 TCT	40 TCT	50 TCT
Al-1 % Cu	TCT in FES	H_μ, *MPa* ΔH_μ, *MPa*	226 -	269 43	290 64	320 94	294 68	274 48
	TCT	H_μ, *MPa* *n*	235 2,05	267 2,01	281 1,95	294 1,92	308 1,88	277 1,85
A1-2 % Cu	TCT	H_μ, *MPa* ΔH_μ, *MPa*	453 -	412 41	498 45	399 54	372 81	330 123
A1-3 % Cu	TCT in FES	H_μ, *MPa* ΔH_μ, *MPa*	400 -	425 25	567 167	759 359	690 290	625 225
	TCT	H_μ, *MPa* ΔH_μ, *MPa* *n*	405 - 2,10	508 103 2,05	596 191 2,00	700 295 1,96	713 308 1,93	725 320 1,93
A1-4 % Cu	TCT in FES	H_μ, *MPa* ΔH_μ, *MPa* *n*	421 - 2,14	602 18 2,07	735 314 1,87	823 402 1,68	785 364 1,67	501 80 1,69
	TCT	H_μ, *MPa* ΔH_μ, *MPa* *n*	420 - 2,14	530 171 1,99	629 209 1,96	768 348 1,92	800 380 1,95	786 366 1,88

Table 4.6

Dependence of microhardness, increase in microhardness ΔH_μ and Mayer index of *Al – Cu – Zn*, *Al – Zn* alloys on the number of thermocycles

Alloy	Heat treatment	Measured size	0 TCT	5 TCT	10 TCT	20 TCT	40 TCT	50 TCT
Al-6 Zn-4 Cu	TCT	H_μ, *MPa* *n*	460 2,14	590 1,95	780 1,83	800 1,74	750 1,79	745 1,77
	TCT in FES	H_μ, *MPa* ΔH_μ, *MPa* *n*	181 - 2,06	200 19 2,00	231 50 1,88	286 105 1,83	285 104 1,84	290 109 1,85
Al-3 % Zn	TCT	H_μ, *MPa* ΔH_μ, *MPa* *n*	190 - 2,06	209 19 1,98	230 40 1,91	256 66 1,76	278 88 1,80	280 90 1,79
Al-4 % Zn	TCT in FES	H_μ, *MPa* ΔH_μ, *MPa* *n*	201 - 2,08	251 50 1,93	292 91 1,80	305 104 1,75	300 99 1,75	901 100 1,61
	TCT	H_μ, *MPa* ΔH_μ, *MPa* *n*	190 - 2,08	205 15 1,99	268 78 1,92	290 100 1,85	293 103 1,80	292 102 1,80

value of H_μ with a subsequent increase at 15-17 TCT. Further increase in quantity of thermocycles leads to a decrease in the value of H_μ. The shear modulus f^2 for this alloy behaves similarly.

The analysis of the research results, which are given in Table 4.5, 4.6 makes it possible to adjust the TCT number in such a way as to obtain an increase in mechanical characteristics while maintaining a sufficiently high level of damping properties, to increase the homogeneity of the structure and to reduce the warping of the parts.

5. Conclusions

1. Thermal cycling leads not only to the formation of high density disloca-tions in alloys, but also to their redistribution into polygonal walls. This is due to the fact that the available impurities, their complexes or separate dispersed allocations significantly block the newly formed dislocations and the already formed substructure, and thus increase its thermal stability and increase the heat resistance of the material. At the same time, as the strength characteristics increase, the damping properties are not significantly lost.

2. The intensity of the manifestation of substructural effects depending on the number of thermocycles has an oscillatory character with an oscillation period of 25-30 thermocycles after thermocycling and 12-15 after thermocycling under load. They stabilize after 50-60 TCT.

3. Thermocycling of dispersion-hardening alloys in a loaded state leads to the acceleration of the achievement of a more strengthened state and extension of the interval of preservation of increased operational characteristics of materials. A correlation was established between the nature of the manifestation of the internal friction during the transition of materials from the metastable to the equilibrium state and the change in their strength properties. Correspondence between the type of substructure, the shear modulus and the value of microhardness was revealed.

4. The nature of the change in T_c depending on the number of TCT in the FES correlates with the change in the tangent of the angle of inclination of the background ADIF $(tg\theta)$, which characterizes the intensity of dislocation separation from the anchoring points, as well as the second critical amplitude of deformation ADIF $(\gamma_{cr.2})$, since an increase in T_c and $\gamma_{cr.2}$ and decrease $tg\theta$ characterizes growth elastic limits of the material.

5. Application of thermocycling under load is possible not only for materials made of dispersion-hardening alloys, which serve as raw materials for engineering and industry, but also for finished parts and technical structures made of them. This will simplify the processing technology, reduce energy consumption and allow to obtain a significant economic effect.

References:

1. Zuzyak P.M., Bilyuk A.I., Khodak V.I., Kaminskys O.S., Shyrokov O.V. (2002). Regularities of the behavior of the mechanical characteristics of Al-Cu and Al-Zn systems in the process of the substructure. *Materials Science*, vol. 38(3), pp. 463–466. DOI: 10.1023/A:1021754607379

2. Lavrentiev V.I. (1997). Mekhanizm pohlynannia enerhii vnutrishnikh napruh v kompozytsiinomu materiali [The mechanism of energy absorption of internal stresses in a composite material]. *Metalofizyka i novitni tekhnolohii – Metallophysics and the latest technologies,* vol. 4.

3. Mordiuk B.M. (2012). *Zakonomirnosti strukturoutvorennia ta kinetyka deformatsiinykh protsesiv u metalevykh materialakh pry kombinovanykh vplyvakh iz zastosuvanniam ultrazvuku*: avtoref. dys. dokt. fiz.-mat. nauk [Patterns of structure formation and kinetics of deformation processes in metallic materials under combined effects with the use of ultrasound: autoref. thesis dr. physics and mathematics of science]. K., 38 p.

4. Biliuk A.I., Karbivskii O.F., Lysiy M.V., Savulyak V.I. (2017). Impact of termocycling on aluminum alloy polygonal structure. Tehnomus, Romania, pp. 117–122.

5. Kohler J.S. (1952). Imperfections in Nearli Perfect Cristals / Ed. by W. Shockley et al Wiley. New York, pp. 197–212.

6. Granato A.V., Lucke K. (1981). Dislocation Dinamics. *J. Ahhl. Phys.,* vol. 27, no. 6, pp. 583–593; vol. 52, no. 12, pp. 7136–7142.

7. Asano S. (1870). Theory of nonlinear damping due to dislocation hysteresis. *J. Phys. Soc. Japan,* vol. 29, no. 4, pp. 952–963.

8. Alefeld G., Filloux J., Harper H. (1973). Dislocation Dinamics / Ed. by A.R. Rosenfeld et al. McGraw-Hill. New-York.

9. Lebediev A.B. (1993). Vnutrishnie tertia pry kvazistatychnomu deformuvanni krystaliv [Internal friction during quasi-static deformation of crystals]. *FTT*, vol. 35, no. 9, pp. 2305–2341.

10. Golovin S., Puskar A. (1992). *A. J. Appl. Phys*., vol. 3, pp. 1–11.

11. Tien J.K., Copley S. (1971). Lottice defects in guenced metals. *Met. Trans*, vol. 2, no. 11, 215 p.

12. Kaiser G., Pechhoid W. (1969). *Acta Men,* vol. 17, no. 4, pp. 527–537.

13. Zasymchuk E.Ie., Zasymchuk V.I., Hontareva R.H. ta in. (2007). *Harmonichnyi analiz substrukturnykh parametriv deformovanykh metaliv* [Harmonic analysis of substructural parameters of deformed metals]: Dop. NAN Ukrainy, no. 10, pp. 91–95.

14. Blaha H. Langeneckar B. (1955). Naturwissenschaften, vol. 42, no. 20, pp. 556–556.

15. Biliuk A.I., Zuziak P.M., Buntar O.H. (1997). Evoliutsiia struktury dyspersiino-tverdiiuchykh splaviv pislia termotsykliuvannia pid navantazhenniam [Evolution of the structure of dispersion-hardening alloys after thermal cycling under load]. *Visnyk Vinnytskoho politekhnichnoho instytutu – Bulletin of the Vinnytsia Polytechnic Institute,* no. 3, pp. 110–115.

16. Postnikov V.S., Belikov A.M., Zolotukhin Y.V. (1967). Vplyv tsyklichnykh nahrivan i okholodzhen na frahmentnu strukturu monokrystaliv aliuminiiu y kadmiiu [Effect of cyclic heating and cooling on the fragment structure of single crystals of aluminum and cadmium]. *FMM*, vol. 23, no. 1, pp. 173–176.

17. Baker G.S., Carpenter S.H. (1967). *J. Appl. Phys*, vol. 38, no. 4, pp. 1586–1591.

18. Kaiser G. Z. (1968). Metallkunde, vol. 59, no. 7, pp. 534–546.

19. Peres S., Delorme J., Pegium P., Cobin P. (1967). The continuons of clamping at contant amplituge. *J. Sci. Instrum*, vol. 44, pp. 69–72.

20. Rivand T., Riviere Z., Grilhe G. (1972). Energie de liaison Zacune-atome de zine dans des alliages Al-Zn dilues. *Scr. Met*, vol. 16, pp. 65–70.

21. Substrukturnoe uprochnenye metallov y dyfraktsyonnue metodu yssledovanyia: materyalu konf. (1985) / Red. kol.: L.N. Larykov, L.V. Tykhonov y dr. Kyiv: Naukova dumka, 280 p.

22. Lebediev A.B. (1999). Amplitudno-zalezhnyi dekrement modulia pruzhnosti v osnovnykh modeliakh dyslokatsiinoho histerezysu [Amplitude-dependent decrement of the modulus of elasticity in basic models of dislocation hysteresis]. *FTTT,* vol. 41, no. 7, pp. 1214–1221.

23. Baranov A.A. (1974). *Fazovi peretvorennia i termotsykliuvannia metalov* [Phase transformations and thermocycling of metals.]. Kyiv: Naukova dumka, 231 p.

24. Bilyuk A.I., Zuzyak P.M., Khodak V.I., Tomchuk V.I. (1993). Intemal friction of beryllium bronze at termotsikrovanii pod nagruzkoj. *Izvestiya Akademss Naur-seriya Fizicheskaya*, 57.

25. Prokopenko H.I., Voloshko S.M., Kotenko I.Ie. ta in. (2009). Zmina mikrotverdosti aliuminiievoho splavu D16 pislia ultrazvukovoi udarnoi obrobky [Change in microhardness of D16 aluminum alloy after ultrasonic impact treatment]. *Nauk. visti NTUU KPI – Science news of NTUU KPI*, no. 3, pp. 42–46.

26. Koidi Sugimoto (1970). An automatic torsion peudulum for measurement of internal friction and shear modulus. *Met. Inst. Sci. Ind. Res*. Osaka Univ., vol. 27, pp. 61–68.

27. Zuziak P.M., Solonenko V.I., Biliuk A.I., Hel P.V. (1985). Ustanovka dlia vymiriuvannia vnutrishnoho tertia i velychyny deformatsii v zalezhnosti vid velychyny mekhanichnoi napruhy v zrazku [Installation for measuring internal friction and the amount of deformation depending on the amount of mechanical stress in the sample]. *Pratsi VII Vsesoiuznoi naukovo-tekhnichnoi konferentsii po NIS "Informatsiino-vymiriuvalni systemy" – Proceedings of the VII All-Union Scientific and Technical Conference on NIS "Information and Measurement Systems"*. Vinnytsia: VPI, pp. 142–143.

28. Blanter M.S., Golovin I.S., Golovin S.A. (1994). *Mehanicheskaya spektroskopiya metallicheskih materialov* [Mechanical spectroscopy of metallic materials]. M.: MIA, 256 p.

29. Zuziak P.M., Biliuk A.I., Honchar O.V. (1995). *Ustanovka dlia termotsyklichnykh obrobok konstruktsiinykh materialiv v navantazhenomu stani i vymiriuvannia VT* [Installation for thermocyclic processing of structural materials in a loaded state and measurement of IF]. Vinnytsia: VDPI, pp. 63–64.

30. Mozghovyi O.V., Zuziak P.M., Holovin S.A. (1990). *Avtomatychna nyzkochastotna ustanovka dlia vymiriuvannia vnutrishnoho tertia* [Automatic low-frequency installation for measuring internal friction]. Vinnytsia: Vinnytskyi derzhavnyi pedahohichnyi instytut, Dep. V Ukr. NIITI 28.03.90 r., no. 565-Uk90.

31. Shyrlovych A.Kh. (1966). *Dyferenntsialni transformatory i yikh zastosuvannia* [Differential transformers and their application]. Kyiv: Naukova dumka, 196 p.

32. Biliuk A.I., Dumenko V.P., Cherevchuk Yu.O., Balukhata L.O. (2014). Temperaturnyi spektr zatukhannia mekhanichnykh kolyvan konstruktsiinykh materialiv [Temperature spectrum of damping of mechanical vibrations of structural materials]: materialy Mizhnarodnoi naukovo-praktychnoi konferentsii*: Nauchnyi prohress na rubezhe tysiacholetyi* – materials of the International scientific and practical conference*: Scientific progress at the turn of the millennium*. 27.05-05.06.2014. Praha, Education and Science, vol. 21, pp. 63–66.

33. Wert C., Marx J. (1953). A New Method for Determining the Heat of Activation fo RelaxationProcess. *Acta Met*, vol. 1, no. 2, pp. 113–118.

34. Biliuk A.I., Biliuk A.A., Klimov I.I., Chekhovska Yu.S., Vitiuk H.V. (2012). Vyznachennia entalpii aktyvatsii relaksatsiinykh maksymumiv substrukturnozmitsnenoho aliuminiiu v hiperbolichnii systemi koordynat [Determination of the activation enthalpy of relaxation maxima of substructurally strengthened aluminum in the hyperbolic coordinate system]: materialyi Mezhdunarodnoy nauchno-prakticheskoy konferentsii *"Novosti nauchnoy myisli"* 27.10-05.11. 2012. Chekhyia. Praha: Publishing House "Education fnd Science" s.r.o., Dil 21, pp. 32–35.

35. Zuzyak P.M., Bilyuk A.I., Fedorchuk I.I. (1994). Kontrol dislokatsionnoy strukturyi materiala metodom regressionnogo analiza [Control of the dislocation structure of a material by regression analysis]: materialyi 7-y Mezhdunarodnoy nauchno-tehnicheskoy konferentsii *"Dempfiruyuschie materialyi"*. Kirov, pp. 42–43.

36. Kuchma S.M., Kuchma S.N., Starodubov S.Iu. (2012). Rozrobka dyspersiino-tverdiiuchoho elinvaru ta doslidzhennia yoho termopruzhnykh vlastyvostei. *Suchasni tekhnolohii v promyslovomu vyrobnytstvi* [Development of dispersion-hardening Elinvar and research of its thermoelastic properties. *Modern technologies in industrial production*]: Materialy II Vseukr. mizhvuz. nauch.-tekhn. konf, 17-20 kvitnia 2012 r.: u 3-kh ch. / Pod red. O. H. Husaka, V. H. Yevtukhova. Sumy: SumDU, vol. 1, pp. 154–155.

37. Mason W.P. (1976). *Advances in materials research.* Nev York: I. Willey, vol. 8, no. 1, pp. 89–101.

38. Bilous M.V., Braun M.P. (1986). *Fizyka metaliv* [Physics of metals]. Kyiv:Vyshcha shkola, 343 p.

39. Adler Yu.P., Markova E.V., Grabovskiy Yu.V. (1978). *Planirovanie eksperimentov pri poiske optimalnyih usloviy* [Planning experiments in search of optimal conditions]. M.: Nauka, 270 p.

40. Biliuk A.I., Biliuk A.A., Kholod A.B., Krasna A.M., Vitiuk A.V. (2015). Pokhybka eksperymentu pry vymiriuvani spektriv rozsiiuvannia mekhanichnoi enerhii v metastabilnykh materialakh [Experimental error in measuring the spectra of mechanical energy dissipation in metastable materials]. Materialy Mizhnarodnoi naukovo-praktychnoi konferentsii: *Dynamika suchasnoi nauky – 2015. 17.07-25.05.2015*. Bolharyia. Sofiia, Bial HRAD-BH OOD, t. 6.

41. Zuziak P.M., Solonenko V.I.,.Biliuk A.I., Nedybaliuk A.F. (1993). Do pytannia pro pokhybku pry vymiriuvanni vnutrishnoho tertia v metasta-bilnykh strukturakh [To the question of error in measuring internal friction in metastable structures]: materialy pershoi mizhvuzivskoi naukovoi konferentsii "*Nauka – rynkovii ekonomitsi"*. Vinnytsia: VDSI, pp. 198–199.

42. Hordiienko L.K., Zuziak P.M., Stronhin B.H. (1974). Doslidzhennia zalezhnosti vnutrishnoho tertia polihonizovanoho aliuminiiu vid rezhymiv MTO. Mekhanizmy relaksatsiinykh yavyshch v tverdykh tilakh [Research on the dependence of internal friction of polygonized aluminum on MTT modes. Mechanisms of relaxation phenomena in solids]. Kaunas: KPI, pp. 98–104.

43. Zuziak P.M. (1972). *Vnutrishnie tertia substrukturno-zmitsnenoho aliuminiiu* [Internal friction of substructurally strengthened aluminum]: avtoref. dys. kand. fiz.-mat. nauk: 01.04.07. Chernivetskyi derzhavnyi universytet. Chernivtsi, 24 p.

44. Zuzyak P.M. (1988). Pogloschenie uprugoy energii v metastabilnyih metallicheskih sistemah: avtoreferat dissertatsii doktora fiziko-matematicheskih nauk [Absorption of elastic energy in metastable metallic systems: abstract of the dissertation of Doctor of Physical and Mathematical Sciences]. Institut metallofiziki AN USSR. Kiev, 46 p.

45. Stronhin B.H., Zuziak P.M., Sumskyi V.I. (1977). *FTT*. Kyiv-Donetsk: Vyshcha shkola, vol. 7, pp. 81–84.

46. Lysyi M.V., Mozghovyi O.V., Biliuk A.I. (2012). Formuvannia zmitsniuiuchoi substruktury v kompozytsiinykh materialakh na osnovi aliuminiiu [Formation of a reinforcing substructure in aluminum-based composite materials]. *Visnyk VPI*, no. 3, pp. 148–153.

47. Larikov L.N. (1980). *Zalichuvania defektiv v metalakh* [Correction of defects in metals]. Kyiv: Naukova dumka, 289 p.

48. Prokopenko H.Y., Berezyna A.L., Voloshko S.M. ta in. (2010). Zmitsnennia poverkhni splava D16 pry ultrazvukovii udarnii obrobtsi [Zmitsnennia poverkhni splava D16 pry ultrazenkovii udarnii obrobtsi]. *Metalofizyka. i nov. tekhnol – Metallofizyka. i nov. technol.*, vol. 32, no. 3, pp. 397–403.

49. Biliuk A.I., Lysyi M.V., Slobodianyk A.D. (2017). Vplyv termotsyklichnoi obrobky na substrukturne zmitsnennia kompozytsiinykh materialiv z aliuminiievoiu matrytseiu [Effect of thermocycling on substructural strengthening of composite materials with an aluminum matrix]. *Problemy trybolohii – Problems of tribology*, no. 1, pp. 63–67.

50. Biliuk A.I. (1997). *Vplyv termotsykliuvannia v poliakh zovnishnikh napruzhen na formuvannia i stabilizatsiiu struktury dyspersiino-tverdiiuchykh splaviv:* avtoreferat dys. kand. fiz.-mat. nauk: 01.04.07 [The influence of thermal cycling in external stress fields on the formation and stabilization of the structure of dispersion-hardening alloys: abstract of the thesis. Ph.D. physics and mathematics Sciences: 01.04.07]. Chernivetskyi derzhavnyi universytet. Chernivtsi, 19 p.

51. Biliuk A.I., Slobodianiuk V.S., Tkach Ye.A., Redko A.A. (2010). Temperaturna zalezhnist substrukturno-zmitsnenykh aliuminiievykh splaviv [Temperature dependence of substructurally strengthened aluminum alloys]. Materialy 6 Mizhnarodnoi naukovo-praktychnoi konferentsii: *Ostani naukovi dosiahnennia – 2010*. 17-25.03.2010. Sofiia, Bial HRAD-BH OOD, vol. 17, pp. 58–61.

52. Biliuk A.I., Popadiuk O.V., Andrianov V.M., Khodak V.I. (2006). Vplyv velychyny zerna na evoliutsiiu substruktury konstruktsiinykh materialakh na osnovi aliuminiiu [The influence of grain size on the evolution of the substructure of structural materials based on aluminum]. *Druha Mizhnarodna naukovo-praktychna konferentsiia "Dni nauky-2006" (17-28 kvitnia 2006)*. Dnipropetrovsk: Nauka i osvita, pp. 15–18.

53. Biliuk A.I., Dumenko V.P., Cherevchuk Yu.O., Balukhata L.O. (2014). Doslidzhennia substruktury aliuminiievykh splaviv pislia termotsykliuvannia metodom mekhanichnoi spektroskopii [Investigation of the substructure of aluminum alloys after thermocycling by mechanical spectroscopy]. Materialy *Mizhnarodnoi naukovo-praktychnoi konferentsii: Suchasna Yevropeiska nauka: 30.06-07.07.2014*. Velykobrytaniia. Sheffield: science and education ltd, vol. 15, pp. 80–82.

54. Biliuk A.I., Khodak V.I., Zlahoda O.M., Pavliuk B.V. (2004). Substrukturne zmitsnennia splaviv Al-Cu-Zn [Substructural strengthening of Al-Cu-Zn alloys]. *1 Mizhnarodna naukovo-praktychna konferentsiia "Naukovyi potentsial svitu – 2004"*. Dnipropetrovsk: Nauka i osvita, vol. 64, pp. 10–12.

55. Zuziak P.M., Kaminskyi O.S. (2004). Doslidzhennia dyspersiino-tverdiiuchykh splavivAl-Cu-Zn z polipshenymy fizyko-mekhanichnymy vlastyvostiamy shliakhom podviinoho zmitsnennia [Study of dispersion-hardening Al-Cu-Zn alloys with improved physical and mechanical properties by double hardening]. *1 Mizhnarodna naukovo-praktychna konferentsiia "Naukovyi potentsial svitu – 2004". Dnipropetrovsk: Nauka i osvita*, vol. 64, pp. 14–15.

56. Lysyi M.V., Biliuk A.I., Slobodianyk A.D. (2016). Substrukturne zmitsnennia aliuminiievykh splaviv pislia termotsykliuvannia [Substructural strengthening of aluminum alloys after thermal cycling]. *Naukovi pratsi VNTU: Enerhetyka ta elektrotekhnika*, no. 4.

57. Byliuk A.Y., Shyrokov V.V., Byliuk A.A. (2015). Strukturoobrazovanye v dyspersyonno-tverdeiushchykh splavakh posle termotsyklyrovanyia. Oraldy hylym zharshysy [Structure formation in precipitation hardening alloys after thermal cycling. Oraldy gylym zharshysy]. *Uralskyi nauchnyi vestnyk. Nauchno-teoretycheskyi y praktycheskyi zhurnal*. h. Uralsk, Respublyka Kazakhstan, TOO "Uralnauchknyha", no. 19, pp. 34–37.

58. Bilyuk A.I., Klimov I.I., Stachuk N.L. (2012). Vliyanie termotseklirovaniya pod nagruzkoy na strukturoobrazovanie dispersionno-tverdeyuschih

splavov [Influence of thermocycling under load on the structure formation of dispersion-hardening alloys]. *Mezhdunarodnaya nauchno-prakticheskaya konferentsiya "Sovremennyie nauchnyie dostizheniya" 27.01-05.02.2012* Chehiya. Praha, Publishing House: Education fnd Science s.r.o., Dil 24, pp. 65–68.

59. Biliuk A.I. (1999). Vplyv termotsykliuvannia pid navantazhenniam na strukturni zminy dyspersiino-tverdiiuchykh aliuminiievykh splaviv [Influence of thermocycling under load on structural changes of dispersion-hardening aluminum alloys]. *Metallofyzyka y noveishye tekhnolohyy,* vol. 19, no. 6, pp. 78–80.

60. Frantsevych Y.N., Voronov F.F., Bakuta S.A. (1982). *Pruzhni postiini i moduli pruzhnosti metaliv i nemetaliv* [Pruzhni postiini i moduli pruzhnosti metaliv i nemetaliv]. Kyiv: Naukova dumka, 286 p.